Evaporation and water sourcing dominate lake and stream isotopic variability across time and space in a High Arctic periglacial landscape

Pete D. Akers[1], Ben G. Kopec[2], Eric S. Klein[3], and Jeffrey M. Welker[3]

[1]Trinity College Dublin
[2]University of Oulu
[3]University of Alaska Anchorage

September 11, 2023

Abstract

Rapidly changing climate is disrupting the High Arctic's natural water systems. This disruption demands high quality monitoring of Arctic hydrology to better reconstruct past changes, track ongoing transformations, and assess future environmental threats. Water isotopes are valuable tracers of hydrological processes, but logistical challenges limit the length and scope of isotopic monitoring in High Arctic landscapes. Here, we present a comprehensive isotopic survey of 535 water samples taken in 2018–2019 of the lakes, streams, and other surface waters of the periglacial Pituffik Peninsula in far northwest Greenland. The $\delta^{18}O$, $\delta^{2}H$, and deuterium-excess values of these samples, representing 196 unique sites, grant us unprecedented insight into the environmental drivers of the region's hydrology and water isotopic variability. We find that the spatial and temporal variability of lake isotopes is dominated by evaporation and connectivity to summer meltwater sources, while evaporation determines interannual isotopic changes. Stream isotopic compositions vary in both space and time based on the relative source balance of tundra snowpack meltwater versus surface melt from the nearby Greenland Ice Sheet. Overall, our survey highlights the diversity of isotopic composition and evolution in Pituffik surface waters, and our complete isotopic and geospatial database provides a strong foundation for future researchers to study hydrological changes at Pituffik and across the Arctic. Water isotope samples taken at individual times or sites in similar periglacial landscapes likely have limited regional representativeness, and increasing the spatiotemporal extent of isotopic sampling is critical to producing accurate and informative High Arctic paleoclimate reconstructions.

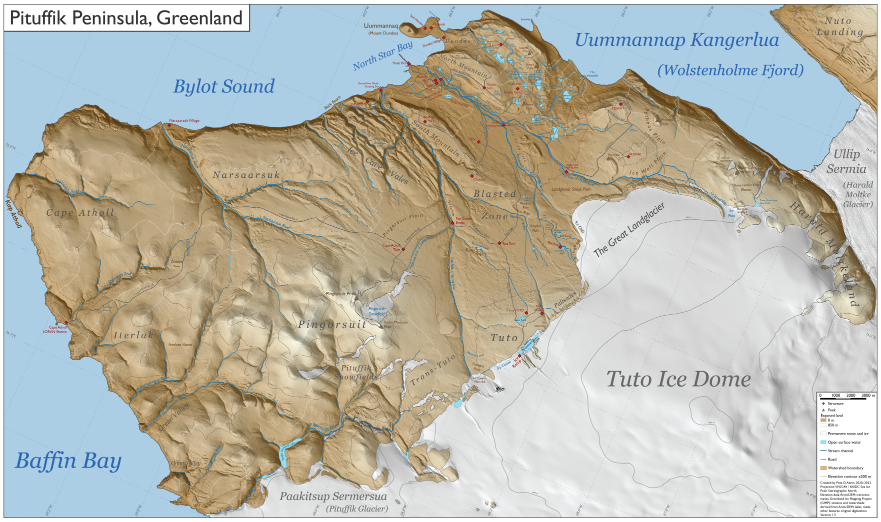
Pituffik Peninsula, Greenland
Bylot Sound
North Star Bay
Uummannaq
Uummannap Kangerlua
(Wolstenholme Fjord)
Nuto Landing
Ullip Sermia
(Harald Moltke Glacier)
Narsaarsuk
Cape Athol
Blasted Zone
The Great Landglacier
Pingorsuit
Iterlak
Pituffik Snowfields
Tuto
Trans-Tuto
Tuto Ice Dome
Baffin Bay
Paakitsup Sermersua
(Pituffik Glacier)

Evaporation and water sourcing dominate lake and stream isotopic variability across time and space in a High Arctic periglacial landscape

Pete D. Akers[1], Ben G. Kopec[2], Eric S. Klein[3], Jeffrey M. Welker[2,4,5]

[1]Discipline of Geography, School of Natural Sciences, Trinity College Dublin, Dublin, Ireland.

[2]Ecology and Genetics Research Unit, University of Oulu, 90014 Oulu, Finland.

[3]Department of Geological Sciences, University of Alaska Anchorage, Anchorage, AK, USA.

[4]Department of Biological Sciences, University of Alaska Anchorage, Anchorage, AK, USA.

[5]University of the Arctic (UArctic), c/o University of Lapland, 96101 Rovaniemi, Finland.

Corresponding author: Pete D. Akers (pete.akers@tcd.ie)

Key Points:

- 535 water isotope samples taken over two years in Pituffik, Greenland, provide exceptional insight into High Arctic isotope hydrology.
- Lake isotopes vary with evaporation and snowpack melt while stream isotopes reflect relative sourcing of snowpack vs. ice sheet meltwater.
- For paleoclimate applications, lakes should be monitored frequently for isotopes for as long as possible as part of a regional lake suite.

Abstract

Rapidly changing climate is disrupting the High Arctic's natural water systems. This disruption demands high quality monitoring of Arctic hydrology to better reconstruct past changes, track ongoing transformations, and assess future environmental threats. Water isotopes are valuable tracers of hydrological processes, but logistical challenges limit the length and scope of isotopic monitoring in High Arctic landscapes. Here, we present a comprehensive isotopic survey of 535 water samples taken in 2018–2019 of the lakes, streams, and other surface waters of the periglacial Pituffik Peninsula in far northwest Greenland. The $\delta^{18}O$, $\delta^{2}H$, and deuterium-excess values of these samples, representing 196 unique sites, grant us unprecedented insight into the environmental drivers of the region's hydrology and water isotopic variability. We find that the spatial and temporal variability of lake isotopes is dominated by evaporation and connectivity to summer meltwater sources, while evaporation determines interannual isotopic changes. Stream isotopic compositions vary in both space and time based on the relative source balance of tundra snowpack meltwater versus surface melt from the nearby Greenland Ice Sheet. Overall, our survey highlights the diversity of isotopic composition and evolution in Pituffik surface waters, and our complete isotopic and geospatial database provides a strong foundation for future researchers to study hydrological changes at Pituffik and across the Arctic. Water isotope samples taken at individual times or sites in similar periglacial landscapes likely have limited regional representativeness, and increasing the spatiotemporal extent of isotopic sampling is critical to producing accurate and informative High Arctic paleoclimate reconstructions.

Plain language summary

The isotopes of water can help us track how rapidly changing climate is disrupting High Arctic water systems, but the challenging Arctic environment has limited the monitoring required to understand its water isotopes. To address this, we collected 535 water isotope samples from lakes, streams, and other waters on the Pituffik Peninsula in northwest Greenland in 2018 and 2019. We found that differences in lake isotopes are mainly due to water evaporation and how connected a lake is to sources of meltwater in the summer. These two factors produce clear patterns in isotopes that we observe over both time and space. The isotopic composition of streams, on the other hand, varies based on the balance of their water that is coming from either melting tundra snow or from melt of the nearby Greenland Ice

Sheet. Our study highlights the varied isotopic makeup of water in the Pituffik area. The information we collected about isotopes is a good starting point for other scientists who want to study how water is changing, not just in Pituffik, but also in the whole Arctic. Our findings tell us that if we only collect water samples once or twice, or only in one place, we might not get the full picture of what is happening with the isotopes across the whole region. To get a better understanding of how the climate is changing in the High Arctic, it's crucial to collect isotopic samples from a wider range of locations and over longer periods of time.

1 Introduction

Anthropogenic climate change is transforming periglacial water systems in the Arctic by shifting the seasonality, intensity, and sources of precipitation, thawing permafrost, increasing surface evaporation, and lengthening snow- and ice-free summers (Bailey et al., 2021; Bintanja & Selten, 2014; Box et al., 2019; Farquharson et al., 2019; Lupascu et al., 2014; Mellat et al., 2021; Vonk et al., 2015). These transformations are greatly disrupting existing ecosystems and biogeochemical cycles (e.g., N. J. Anderson et al., 2017; Bhatt et al., 2017; Buchwal et al., 2020; Gimeno et al., 2019; Hiltunen et al., 2022), as well as threatening long-established livelihoods of indigenous Arctic communities (Hauser et al., 2021; Wesche & Chan, 2010). Despite the Arctic experiencing some of the most rapid climate change on Earth (Serreze & Barry, 2011), Arctic freshwater systems (e.g., lakes, streams, supra-permafrost flow) are lesser studied and monitored than systems in other regions of the world due to their remoteness, harsh environments, and relatively lower magnitude of use by human populations (Linderholm et al., 2018). As a result, this lack of baseline studies and data can make it difficult to quantify how the hydrology of an Arctic region has changed or is currently changing.

Here, we provide one such baseline study through a foundational overview of the hydrological structure and stable isotopic variability of the surface freshwater system across the periglacial Pituffik Peninsula in northwest Greenland. The stable isotopic composition of water (discussed here through δ^{18}O and δ^{2}H, where $\delta = \frac{R_{sample}}{R_{standard}} - 1$ and R is the measured ratio of rare to abundant isotopologue, and through deuterium-excess (*dxs*), where $dxs = \delta^{2}\text{H} - 8 * \delta^{18}\text{O}$) can assist in quantifying the fundamental properties and processes of the Arctic environment by serving as key environmental tracers for water throughout its hydrological cycle history (Craig, 1961; Dansgaard, 1964; Gat, 1996; Gonfiantini, 1986; Rozanski et al., 1993). This tracing is possible because water molecules containing heavier isotopes of oxygen and/or hydrogen are discriminated against through kinetic fractionation during phase transitions from solid to liquid to vapor and favored during the reverse of these transitions. This fractionation leads to a strong linear relationship in oxygen and hydrogen isotopic ratios in precipitation that is described globally with the global meteoric water line (GMWL) where $\delta^2H = 8 * \delta^{18}O + 10$ ‰ (Craig, 1961) and locally with local meteoric water lines (LMWL) (Putman et al., 2019; Rozanski et al., 1993). Additionally, diffusion across a humidity gradient during evaporation can slightly favor the vapor phase enrichment of H^2HO relative to the more slowly diffusing $H_2{}^{18}O$ molecule, and the impact of this nonequilibrium process can be quantified through the second-order isotopic parameter of *dxs* (Craig & Gordon, 1965; Merlivat & Jouzel, 1979). For open bodies of water that experience sustained evaporative losses, this nonequilibrium process means that their δ^2H vs. $\delta^{18}O$ values will plot along a local evaporation line (LEL) that falls below the GMWL and LMWL in δ^2H–$\delta^{18}O$ space (i.e., the slope of the δ^2H vs. $\delta^{18}O$ relationship will be lower than the slopes of the GMWL and LMWL).

Due to these isotopic processes, the stable isotopic ratios and *dxs* values of two identical source waters will diverge from each other as they experience different histories of evaporation, condensation, and transportation. As a result, water isotopic compositions have been harnessed with great success in the Arctic to identify moisture sources of precipitation and water vapor (e.g., Akers et al., 2020; Bailey et al., 2021; Bonne et al., 2014; Kopec et al., 2019; Mellat et al., 2021), estimate lake water balances (e.g., L. Anderson et al., 2013; Arp et al., 2015; Cluett & Thomas, 2020; Gibson & Reid, 2014), examine plant ecophysiology (e.g., Jespersen et al., 2018; Muhic et al., 2023), and reconstruct past climate (e.g., Daniels et al., 2021; Lasher et al., 2017; MacGregor et al., 2020; McFarlin et al., 2019). Provided that the isotopic ratios of an initial water source supply are known or can be estimated, the isotopic ratios of environmental waters in lakes, streams, and the subsurface can also be used to track water movement and calculate hydrological budgets across the landscape (e.g., Bowen et al., 2018; I. D. Clark & Fritz, 1997; Gibson et al., 2016; Kendall & McDonnell, 1998; Noor et al., 2023; Wilcox et al., 2022).

This study presents isotopic data for over 500 individual water samples from 200 unique sites across the Pituffik Peninsula along with an associated hydrological geospatial database. Together, our data offer a spatially and temporally detailed snapshot of a largely intact High

Arctic hydrological landscape in the early 21st century. Through this nearly complete systematic sampling of Pituffik water bodies over two consecutive summers, we provide a comprehensive baseline dataset of the lakes, streams, and other surface waters in our large study region (>800 km^2) that can serve as a high-quality reference for contemporary and future circumpolar studies. We use these survey data to determine the environmental drivers of lake and stream isotopes in the Pituffik freshwater system for broader application to analogous water systems across the Arctic.

Many paleoenvironmental studies using natural archives of oxygen and hydrogen isotopes in sediments must assume typical water isotopic values from local water isotopic monitoring to reconstruct past environmental changes (e.g., McFarlin et al., 2019; Sauer et al., 2001; Verbruggen et al., 2011). However, the logistical challenges of Arctic field work often force these assumptions to be based on limited monitoring data, and inferences and conclusions made in light of such data risk inaccuracy and misinterpretation if the monitoring data were not truly representative of local and/or regional isotopic norms. Therefore, the comprehensive nature of our Pituffik isotopic survey gives light to the general natural variability that exists in Arctic surface water isotopic systems across both time and space, and we use this knowledge to advise best practices for paleoenvironmental researchers working in similar environments. Overall, our insight into the isotopic variability of this High Arctic periglacial water system offers great potential for researchers using isotopic proxies for reconstructing both past and current environmental change as well as providing future researchers a reference point to examine how much the environment will have changed since the early 21st century.

2 Geographic overview of the Pituffik region

Our study focuses on the "Pituffik region" of northwest Greenland which we define here as synonymous with the Pituffik Peninsula and its nearby offshore waters (Figure 1). A full understanding of the modern hydrology of the region must be grounded in the context of its environmental and human history. The region covers roughly 880 km^2 of ice-free land bounded by the Greenland Ice Sheet (GrIS) to the east, Baffin Bay and Bylot Sound to the west, and Uummannap Kangerlua (Wolstenholme Fjord) to the north (76.25–76.60 °N, 67.60–69.70 °W). This region is also commonly referred to as the "Thule area" in reference to the original Danish placename and a subsequent local United States military base. Place names throughout this text will be given in the following priority as known: indigenous Greenlandic names first (Oqaasileriffik, 2022), followed by common English and Danish names, and finally informal names assigned by the authors to features with no known existing names.

The landscape of the Pituffik Peninsula has long been noted for its numerous distinctive landmarks, including the flat-topped Uummannaq (Mount Dundas), the easily accessed "Tuto" margin of the GrIS, and the broad, formerly ecologically productive valley now filled by Pituffik Space Base (Figure 1a). The southern and western parts of the peninsula consist of relatively gently sloped uplands culminating in the 815 m Pingorsuit massif, while the northern part of the peninsula near the military base has many broad ridges, steep-faced outcrops, and lakes interspersed on a wide plain that steadily rises eastward toward the local Tuto ice dome of the GrIS (Davies & Reitzel, 1963). The Tuto dome itself covers ≈1000 km^2 with maximum elevations over 1000 m. Although connected to the main GrIS, the Tuto dome has a largely independent mass balance regulated by local precipitation, extensive summer surface melt, and discharge through several large marine terminating glaciers. Climate change in recent decades have seen substantial thinning of the Tuto dome, shrinking and loss of permanent snowfields across the peninsula, and tidewater glacial retreat of 1–5 km (Copernicus, 2019; Korsgaard et al., 2016; Müller et al., 2021).

The Pituffik region holds an outsized role in the ecology and history of the Greenlandic and Canadian High Arctic. Due in part to its proximity to the North Water polynya, Pituffik supports immense seabird colonies in Baffin Bay coastal valleys and hosts important habitat for large populations of marine mammals and waterfowl (Burnham et al., 2014; Hastrup et al., 2018; Heide-Jørgensen et al., 2016; Mosbech et al., 2018). This biological productivity has drawn humans to the region for thousands of years (Gronnow, 2016; Hastrup et al., 2018), and the Thule culture, ancestral to modern Inuit and Greenlandic peoples, was first formally described from excavations conducted on the northern coast of the Pituffik Peninsula (Jenness, 1925). Today, the surface across most of the entire peninsula is covered by coarse glacial deposits with sparse polar desert vegetation (Corbett et al., 2015; Funder, 1990; Nichols, 1953). More lush vegetation occurs in low-lying moss wetlands and within the seabird colony valleys (Cuyler et al., 2022; Mosbech et al., 2018) while vast stretches of boulder and cobble outwash plains that extend out from the GrIS margin support only lichens (Davies & Reitzel, 1963).

In the 1950s, Pituffik gained global importance and notoriety with the American construction of Thule Air Base (now Pituffik Space Base) as part of the Cold War militarization of the Arctic. Over 10000 American personnel were present for the initial construction and occupation of the base, and at this time these soldiers and contractors comprised over one quarter of the total population of Greenland. Construction of the base ushered in a period of forced relocations of indigenous communities, environmental degradation, and novel resource access that has major ongoing impacts on Greenlandic culture and home rule debates today (Colgan et al., 2016; Eriksson et al., 2004; Gronnow, 2016; Takahashi, 2019).

The presence of the military base has also made the Pituffik Peninsula a focal point for environmental studies of the Arctic and cryosphere. American military funding in the early Cold War sent engineers, geologists, and climatologists to Pituffik to test experimental methods of boring into permafrost and the GrIS (Nichols, 1953; Ries, 2012; Schytt, 1955; Swinzow, 1962). While the clandestine goal of ice sheet-spanning tunnel networks to house nuclear weapons failed (Amstrup, 1997; Petersen, 2008; Weiss, 2001), the studies laid much of the foundational research for modern ice core drilling and paleoclimate studies (E. F. Clark, 1965; Dansgaard et al., 1969; Hansen & Langway, 1966). More recently, the logistical ease of transport to the base coupled with housing and entertainment infrastructure has made Pituffik an attractive option for hosting multiyear environmental research projects (e.g., Akers et al., 2020; Burnham et al., 2014; Corbett et al., 2015; Jespersen et al., 2022; Leffler & Welker, 2013). Our research builds off this extensive foundational knowledge and used the extensive local infrastructure of housing and roads to achieve our dataset’s impressive spatiotemporal extent.

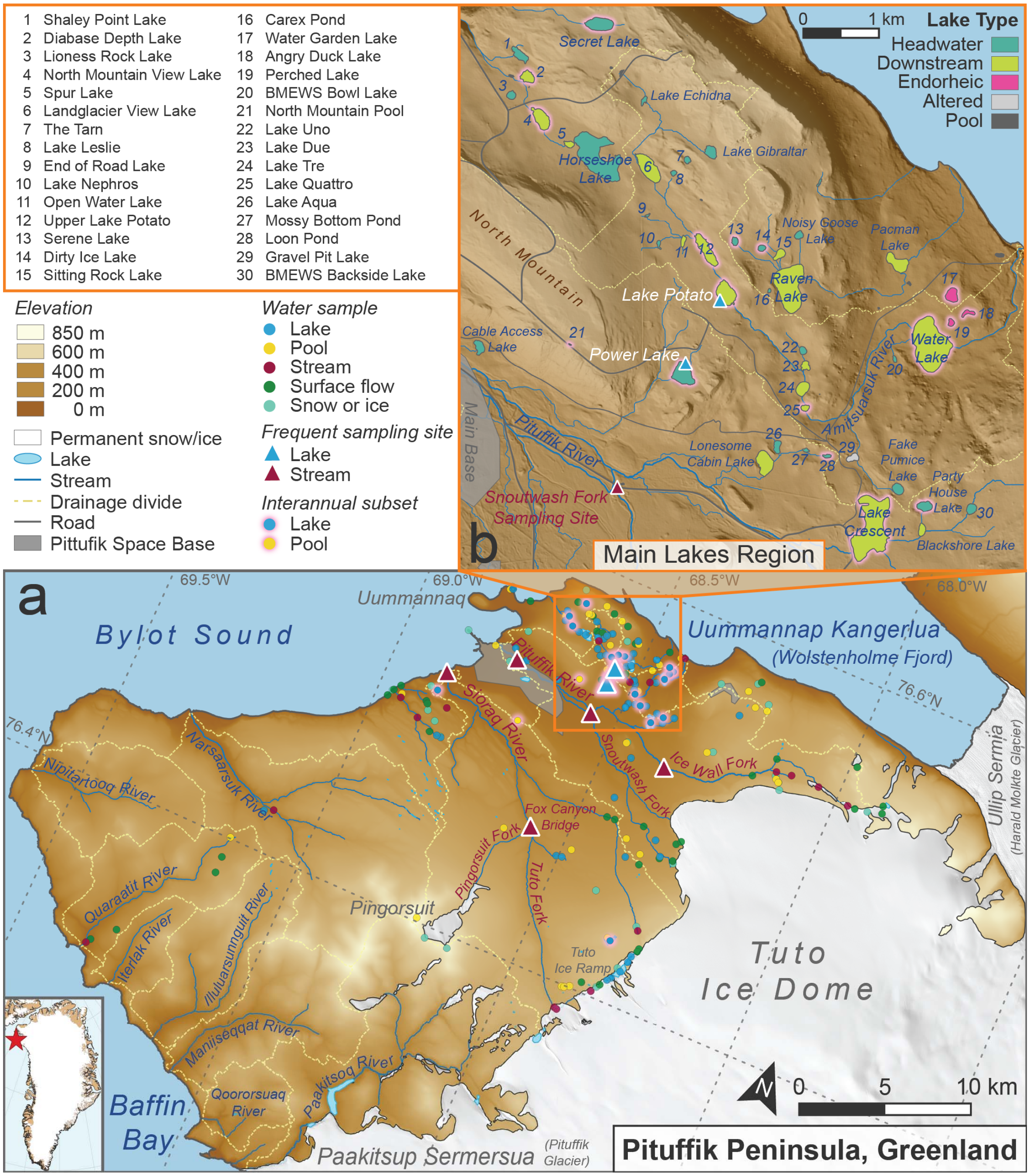

Figure 1. Map of the Pituffik region of northwest Greenland. Across the full Pituffik Peninsula (a), water sample sites (circles) are colored according to the type of surface water sampled. The eight lake and stream sites frequently sampled for temporal study are shown by triangle icons. Note that samples for the Pingorsuit and Tuto Forks of the Sioraq River were both taken at the Fox Canyon Bridge where the forks join. Lakes and pools sampled during each of the three main sampling periods for interannual analysis are highlighted by pink. The main lakes region is given additional focus (b) to show the spatial distribution of the main

lakes and their lake type categories. Note that no vale or proglacial lakes are present in the main lakes region. Geospatial data used to construct the map includes ArcticDEM (Porter et al., 2019), ice and ocean masks from the Greenland Ice Mapping Project (Howat, 2019), and place names from the Language Secretariat of Greenland (Oqaasileriffik, 2022).

3 Materials and Methods

3.1 Hydrological survey and geospatial database

We created a new hydrological geospatial database at a previously unavailable resolution and detail for the Pituffik region to support our isotopic field sampling. Field observations of the regional hydrology made during the 2018 and 2019 sampling campaigns provided the foundation and ground-truthing for later geospatial analyses. These analyses and map creations were performed through QGIS with *GRASS*, *GDAL*, *SAGA*, and *Point Sampling* packages. Drainage basins and stream networks for the Pituffik region were extracted from the 2 m ArcticDEM (PGC, 2019; Porter et al., 2019) with *GRASS* flow and drainage tools. Lakes and roads were hand digitized based on both Sentinel 2 satellite imagery from 15 August 2019 (Copernicus, 2019) and orthorectified aerial imagery from summer 1985 (Korsgaard et al., 2016). Each lake was assigned a lake type category (from the list of endorheic, headwater, downstream, vale, proglacial, and altered) based on its hydrological connectivity and environmental character observed in the field.

Geographic coordinates for water sampling sites and notable landmarks were taken with an iPhone 7 GPS and later validated for accuracy with the satellite and aerial imagery. Elevations for sampling sites were extracted from the 2 m ArcticDEM using validated site geographic coordinates. For each lake, the distances to the ocean and to the GrIS (i.e., the Tuto dome margin) were calculated in QGIS as the minimum horizontal distance between the centroid of each lake and the perimeter of the polygons enclosing the ocean and the ice sheet, respectively, using ocean and ice masks defined from the Greenland Ice Mapping Project (GIMP) (Howat, 2019; Howat et al., 2014). Perennial snow patches were excluded from the GIMP ice mask for this calculation to ensure that distances were to the actual GrIS margin.

3.2 Field sampling

Field sampling of Pituffik surface waters occurred when we were present at Pituffik in June–August 2018, November 2018, and July 2019. The samples sort into seven categories based on their source origin: lakes (standing body of water > 1000 m^2 surface area with a defined shoreline), pools (shallow standing body of water < 1000 m^2 surface area and/or no defined shoreline), streams (continuous summer flow in a defined channel), surface flow (sheet flow/seeps with undefined channels and also very small intermittent streams), snow or ice (including aged remnant snow patches, remnant lake ice, glacial/multiannual ice, and frost), and both rain and snow precipitation events. We divide the summer sampling into three main periods: early summer 2018 (14 Jun–18 Jul), late summer 2018 (19 Jul–23 Aug), and mid-summer 2019 (19 Jul–01 Aug). Sampling in November 2018 was restricted to precipitation events and the local snowpack as all lakes, streams, and other surface waters were frozen or dry. Aside from the local military road network, no marked trail systems exist in Pituffik, and sample site discovery and access was gained through overland hiking across the tundra and boulder outwash plains to geographic coordinates identified through satellite imagery.

Water sampled for isotopes was collected in clean and dry 50 ml plastic centrifuge tubes that were closed tightly and sealed with Parafilm. For lakes and pools, water was sampled 10–20 cm below the surface from a downwind shore. For streams, water was collected for 3–10 times the duration required to fill the tube (~5–30 s). For snow and ice sampling, enough snow or ice was collected to fill the tube whereupon it was sealed and allowed to melt at ambient air temperature. Rain and snow precipitation were sampled as soon as possible after each event ended from accumulation in clean rain gauges or, in the case of some snow events, in bowls or the ground surface outside building 345 on Pituffik Space Base. For all water samples, tubes were filled as full as possible to limit evaporation into the head space and shipped in liquid state for storage and later aliquot sampling. Monthly GNIP precipitation data collected at Thule Airport between 1966 and 1971 (IAEA/WMO, 2022) were downloaded to construct a LMWL for isotopic comparison. Meteorological data for 2018–2019 were collected through weather stations at two sites on the military base (Muscari, 2018; USAF, 2019). Daily potential evapotranspiration (PET) rates for Pituffik were downloaded from a 0.1° spatial resolution dataset modeled with ERA5-Land reanalysis data (Singer et al., 2021).

Although most lakes and streams were only sampled once each sampling period due to remoteness, we chose two lakes and six stream sites that were easily accessed by road to frequently sample (i.e., 10–18 times each) (Figure 1). This frequent sampling provided more detailed insight into isotopic evolution of the lakes and streams over time. The sampling of these eight sites in 2018 covered most of the thawed summer season from 14 June through 23 August while sampling in 2019 spanned 15 days from 17 July through 01 August. The two frequently sampled lakes, Lake Potato and Power Lake, are located only 1 km apart with similar surface elevations (190 and 178 m a.s.l., respectively) and surface areas (60289 and 59537 m^2, respectively) but belong to different watersheds. Additionally, Lake Potato is the fourth lake in a chain along the Amitsuarsuk River (Potato Creek) and has a large upstream drainage basin of 4.9 km^2 while Power Lake is a headwater lake with a small 0.3 km^2 drainage basin and limited outflow. Together, these two lakes are broadly representative in type of most non-proglacial lakes in the Pituffik region.

The six frequently sampled stream sites were equally split between the Pituffik River and Sioraq River, which together drain 29% of the ice-free Pituffik region. Both these streams receive meltwater directly from the Tuto dome of the GrIS but also drain wide expanses of tundra and some perennial snow patches. To examine the potential effect of different headwater sources on stream isotopes, we regularly sampled each stream mouth as well as two major upstream forks for each stream: the Ice Wall and Snoutwash Forks for Pituffik River, and the Tuto and Pingorsuit Forks for Sioraq River. The Ice Wall, Snoutwash, and Tuto Forks all originate at different points along the GrIS margin, but the Pingorsuit Fork originates in a permanent montane ice field separate from the GrIS.

Stable isotope ratios ($\delta^{18}O$ and δ^2H) of 2 ml aliquots were measured at the University of Oulu using a Picarro L2130-i isotope and gas concentration analyzer fitted with an autosampler (A0325) and vaporizer unit (A0211). Reference standards of USGS-45 ($\delta^{18}O$: −2.2 ‰, δ^2H: −10.3‰) and USGS-46 ($\delta^{18}O$: −29.8 ‰, δ^2H: −235.8 ‰) were used within each analytical run to monitor and correct for instrumental drift as well as to calibrate to the SMOW-SLAP scales for reporting. Each water sample was measured seven times with data from the first three measurements discarded to limit potential memory effects. Samples were reanalyzed if the standard deviation exceeded 0.3 ‰ for $\delta^{18}O$ or 3 ‰ for δ^2H, or if the reference standard used in the run differed from the known isotope value by greater than ±0.2 ‰ for $\delta^{18}O$ or ±2 ‰ for δ^2H. These standards span the full isotopic range of our Pituffik water samples except for seven winter snow events and two snowpack samples. Although these snow samples' involvement in further analyses was limited, we are still confident of their values as the calibrated Picarro instrument linearly infers isotopic ratios to values well below any of our samples (Casado et al., 2016). Based on within-run replicate analyses of standard waters, mean analytical precision was ±0.1 ‰ for $\delta^{18}O$ and ±0.6 ‰ for $\delta^{2}H$. Eighteen water samples were flagged during quality control for having visibly cracked and/or leaking vials after transport, and these samples, along with two tap water samples taken on Pituffik Space Base, were not included in further analyses.

3.3 Spatial and temporal analyses

Beyond a basic overview of all surface water isotopic variability across the Pituffik landscape, we focused our study on the spatial and temporal variability of lake and stream isotopic compositions. Because the isotopic composition of non-frozen surface waters is constantly evolving in response to changes in precipitation, runoff, and evaporation (Gibson et al., 1998; Gibson & Reid, 2014), any attempt to compare water isotopes spatially across multiple lakes and/or streams requires that the water samples are all collected in as short of a time window as possible. Our spatial study of lake isotopic compositions therefore focused on 63 lakes sampled during the two-week period in mid-summer 2019 because this dataset represents nearly all Pituffik lakes while also having a short sampling period that limits temporal isotopic impacts.

The spatial analysis first focused on whether lake type categories assigned to each lake have a relationship with lake isotopic compositions based on isotopic distributions per lake type category and hierarchical cluster analysis of lake $\delta^{18}O$ and *dxs* values. Following the lake type results, we performed multiple regression and LASSO regression between the three isotopic variables and six lake parameters of surface elevation, surface area, watershed area, distance from nearest GrIS margin, distance from nearest ocean coast, and day of year sampled. We restricted this analysis further from the lake type analysis dataset to include only 42 headwater and downstream lakes located in the main lakes region. By narrowing our analysis to this subset of lakes that share common hydrological settings and similar isotopic compositions, the subtle influences of lake parameters could emerge beyond the wide isotopic differences that span lake type categories. Our study on the spatial variability of streams was more limited and focused on comparing the isotopic composition of samples from the three stream networks of the Pituffik, Sioraq, and Amitsuarsuk Rivers.

The temporal analysis of lake isotopes examined isotopic evolution over the 2018 summer season as well as between the summers of 2018 and 2019. For these analyses, we used both the frequently sampled Lake Potato and Power Lake data and a multi-annual subset of 18 lakes and 2 pools that were sampled for water isotopes during each of the three main sampling periods. Finally, we also examined the temporal variability of stream water isotopes using the frequently sampled data from three sites each on the Pituffik and Sioraq Rivers. Both lake and stream isotopic changes over time were compared with local weather records (Muscari, 2018; USAF, 2019) and modeled PET (Singer et al., 2021) to interpret the roles of key climatological parameters might play in the observed isotopic changes over time.

Statistical analyses and figure creation were performed in RStudio using the R language with packages *ape, broom, clock*, *cowplot*, *dendextend, gridExtra*, *ggdendro, glmnet, gridgraphics, ncdf4, raster, reshape2, Rmisc,* and *tidyverse,* and figures were aesthetically adjusted in Adobe Illustrator. Uncertainties for statistical values are given as 95% confidence intervals unless otherwise noted.

4 Results

4.1 Hydrological survey and geospatial database

The geospatial data resulting from our hydrological survey has been made openly available as a geospatial database (Akers et al., 2023b). Individual vector files in the database include points of field observations and placenames, polylines of elevation contours, roads, stream networks, and drainage divides, and polygons for lakes, lake drainage basins, stream drainage basins, ice-covered land, and ice-free land. Raster data of digital elevation models (PGC, 2019), aerial imagery (Korsgaard et al., 2016), and satellite imagery (Copernicus, 2019) for the Pituffik region is not provided in the geospatial database due to large file sizes, but can be downloaded from their original, openly available sources. Using the geospatial database, we created a hydrology and surface features map for Pituffik that is offered as both a large poster

(Figure S1) and as a multipage atlas (Akers et al., 2023b). A general overview of the Pituffik surface water landscape as informed by our hydrological survey results follows.

The surface drainage system of the peninsula is dominated by four main river and stream networks (hereafter referred to collectively as streams) that each drain over 100 km^2. Together, these four basins of the Sioraq (South River), Paakitsoq (Pituffik Glacier River), Pituffik (North River), and Narsaarsuk Rivers cover half of the non-glaciated land surface of the Pituffik region. An additional six streams (Maniiseqqat, Illuluarsunnguit, Quaraatit, Nipitartooq, Qoororsuaq, Iterlak, and Amitsuarsuk Rivers) drain basins each larger than 10 km^2 while numerous smaller basins directly drain coastal lands into the ocean. Of the ten largest stream basins, only three directly drain meltwater from the GrIS: the Pituffik River, Sioraq River, and Paakitsoq River. Outside of the larger streams, well-defined channels are rare across the landscape with most local drainage occurring as sheet flow across the surface or subsurface flow through the coarse rocky active layer.

The Pituffik hydrological system is highly reactive to the thaw of waters frozen in snowpack, glacial ice, and surface waters brought on by both typical seasonal warming and irregular short-term heat events. Although Pituffik surface waters are dry and/or frozen for 7–8 months of the year, the melting of the winter snow cover in May–June (Figure S2) brings an initial period of high surface flow and numerous small pools left in depressions across the tundra. These pools drain in 2–3 weeks as summer progresses and the active layer deepens, and summer flows for streams not sourced at the GrIS are sustained largely by melting residual snow patches (Figure S3). For the three stream basins linked to the GrIS, water discharge often exhibits two seasonal peaks (Csank et al., 2019). After the initial early summer pulse from the melting of the winter tundra snowpack, streamflows also increase in later summer as a result of surface melting of the GrIS and its snow cover. During extreme heat events, such as in 2012 and 2019 (Cullather et al., 2020; Nghiem et al., 2012; Sasgen et al., 2020), massive volumes of glacial runoff greatly swell the streams sourced at the GrIS and can threaten local infrastructure (Figure S3b, d).

The Pituffik region also hosts numerous permanent lakes and ponds (hereafter referred to collectively as lakes) typically formed in Late Pleistocene moraines and till (Figure S4). Around 70 non-proglacial lakes across the peninsula have a surface area greater than 5000 m^2, and several very large proglacial and ice-dammed lakes occur along the margins of the Tuto ice dome and its outlet glaciers. In total, approximately 3.8 km^2 of the Pituffik surface is covered by lakes, of which 2.4 km^2 are non-proglacial. These lakes are typically frozen over between September and April, with ice-out beginning in late May to early June (Figure S2, Figure S5). For the largest lakes, ice cover is largely intact through June, and some ice may remain even into August in colder summers. Over half of the region's lakes are clustered in a 23 km^2 zone north of Pituffik River and northeast of the military base which we refer to as the "main lakes region" (Figure 1b). The construction of military buildings and roads have affected some surface drainage and lakes, most notably with the conversion of Lake Crescent into a dammed reservoir (Davis, 1966), but aerial photographs (Figure S6) predating the base's construction show that the vast majority of lakes still retain their natural layout (Historiske Kort, 2023). We could not find indigenous names for Pituffik lakes despite extensive efforts, and only a few lakes have local English or Danish names. We therefore informally assigned most of the lake names in our database.

Across the Pituffik region, we sorted lakes into six lake type categories based on each lake's environmental and hydrological setting: endorheic, headwater, downstream, vale, proglacial, and altered (Figure 1b, Figure 2, Figure S4). We assigned these lake types prior to any isotopic analysis based solely on physical lake characteristics observed during field sampling. Endorheic lakes fill the low points of small enclosed basins with ill-defined shorelines and have no clear inflow or outflow channels, although it is possible that some subsurface water exchange occurs in the active layer above the permafrost. A headwater lake is connected to a fluvial network but has no lake farther upstream, whereas a downstream lake is any lake along a fluvial network that receives upstream water from at least one other lake. Lake fluvial interconnections may be through stream channels or less defined surface and near-surface flow, and blanketing moss is typically extensive along the shores of headwater and downstream lakes and along their connecting drainage routes. Vale lakes are found within rocky steep-sided valleys primarily located south of Pituffik Space Base. Although vale lakes are interconnected by valley drainage systems, they differ from headwater and downstream lakes in their lack of clear shorelines, near absence of any surrounding vegetation, and rugged topographic setting. The proglacial lakes sampled in our study form a connected chain directly in contact with the GrIS margin that are fed by melting glacial runoff and eventually drain into the Sioraq River. Altered lakes either exist only because infrastructure has blocked natural drainage or are natural lakes whose watershed and drainage are so heavily disrupted by human changes that they no longer reflect natural conditions. We assigned one lake type category to each lake based on observations in the field, but we emphasize that these categorizations were personal judgments to sort lakes that may fall along a continuum of types.

Figure 2. Photographic examples of the six lake type categories assigned to Pituffik lakes. Each lake example here exhibits the major defining characters of its lake type. Note in particular (a) the shallow depth and ill-defined shoreline of the endorheic Angry Duck Lake, (b) the vegetated shoreline hydrologically constraining the headwater Carex Pond, (c) the Amitsuarsuk River flowing through the downstream Lake Tre, (d) the lack of vegetation and steep valley (i.e., vale) setting of Rocky Vale Lake, (e) the direct contact of proglacial Iceberg Lake with the GrIS margin, and (f) the exposed former lake bed of altered Gravel Pit Lake which was partially drained through an artificial outlet channel.

4.2 General isotopic summary

In total, we collected 535 samples from 196 unique sites across the Pituffik region, representing 67 lakes, 37 pools, 24 sites along major streams, 50 sites with surface flow, and 57 snow or ice deposits. The $\delta^{18}O$, $\delta^{2}H$, and *dxs* of the samples largely fall within similar ranges regardless of origin type with mean ± 1σ isotopic values for all samples of $\delta^{18}O$: −19.3±3.6 ‰, $\delta^{2}H$: −151±22 ‰, and *dxs*: = +3±9 ‰ (Figure 3a). The isotopically much lighter winter snow precipitation events are an exception to this general similarity. Across the other samples, we observe that lake and pool are generally isotopically heavier than other sample types, while the *dxs* of lakes and pools are on average lower than other types with a substantial skew towards extreme lower values of −10 to −40 ‰. This wide range in Pituffik lake isotopic values is comparable in magnitude to the isotopic range reported from lakes 1300 km south in Kangerlussuaq, Greenland (Cluett & Thomas, 2020; Leng & Anderson, 2003). The mean $\delta^{18}O$ and $\delta^{2}H$ values of streams, surface flow, and snow/ice deposits are similar to our observed rain events and much higher than snow events, but their *dxs* values are intermediate between rain and snow events.

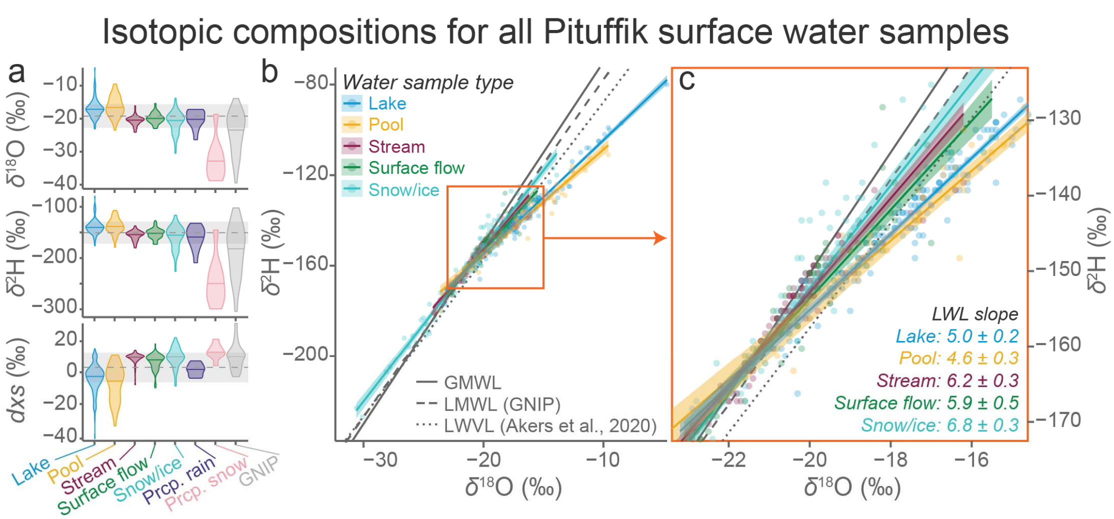

Figure 3. Isotopic compositions of Pituffik surface waters. Violin plots (a) show the distributions of isotopic ratios of Pituffik water samples, grouped by sample source type. Data are plotted so that the maximum width is equivalent between groups, regardless of sample count. The mean isotopic values ± 1 standard deviation of all water samples are shown by the dashed line and gray shaded bar crossing all violins. Within each violin, the

median value per group is shown by a solid horizontal line. GNIP samples are monthly precipitation means collected between 1966 and 1971 (IAEA/WMO, 2022). In (b), linear regressions between $\delta^{18}O$ and $\delta^{2}H$ illustrating local water lines (LWLs) are shown for the different sample source types with shading representing the 95% confidence interval of the regression. The global meteoric water line (GMWL, solid gray), local meteoric water line (LMWL, dashed gray) based on GNIP data (IAEA/WMO, 2022), and local water vapor line (LWVL, dotted gray) (Akers et al., 2020) are shown for reference. The plot in (c) is a magnified version of the area indicated with the orange square in (b), and LWL slope values with 95% confidence intervals are provided for each sample type at lower right. Regressions for precipitation data are provided in Figure S7.

Linear regressions of $\delta^{2}H$ vs. $\delta^{18}O$ (the local water lines, or LWLs) show that different water source types isotopically diverge from the GMWL and the LMWL to different degrees (Figure 3b–c, Table S1). Precipitation events of both snow and rain as well as snow and ice sampled from across the landscape have slopes that are similar to the isotopic reference lines (Figure 3, Figure S7). This similarity is expected for the snow precipitation events and surface snow/ice since they are frozen and therefore have not experienced post-precipitation evaporation. Interestingly, while the slope of the summer rain events is within uncertainty to the LMWL, the rain events have a ≈+5 ‰ $\delta^{18}O$ bias relative to the LMWL (Figure S7). With the limited number of sampled events (n=14), it is not fully clear what is causing this bias. Differences in moisture transport and sourcing due to climate change since the GNIP sampling era may partly explain the offset. Additionally, this bias may also result from minor evaporation occurring during the rain events (as the rain falls through an unsaturated lower atmosphere) or in the rain gauge/bowl before collection.

In contrast, the liquid surface waters of Pituffik all display some degree of isotopic change from evaporation as evidenced by their lower LWL slopes that we interpret as LELs (Figure 3, Table S1). Lakes and pools diverge the most from the LMWL while streams and surface flows diverge less but still noticeably. Theoretically, the intersection of an LEL and the LMWL defines the isotopic values of the initial source water prior to evaporation (Welhan & Fritz, 1977), although this approach has known flaws when the LELs are defined by samples from multiple sources that likely do not share identical initial water isotopic values (Bowen et al., 2018). Acknowledging these limitations, we note that the LELs for lakes, pools, streams, and surface flow all predict very similar initial water isotopic values between −20.0 and

−21.0 ‰ for δ^{18}O and −153 and −160 ‰ for δ^{2}H. These values are slightly higher than the amount-weighted GNIP mean values of −22.5 ‰ and −173 ‰, which could suggest that the surface waters are slightly biased toward summer precipitation. However, we also note that conclusive comparisons are difficult as the Thule GNIP data has several missing months of isotope data, and mean isotopic values for precipitation today may be higher than during GNIP's 1966–1971 collection period due to climate change.

Building off this foundation of Pituffik surface water isotopic compositions, we focused on examining the drivers of isotopic variability in the lake and stream samples across both space and time. We used the pool, surface flow, snow/ice, and precipitation data for environmental context when interpreting the lake and stream isotopes, but deeper examination of their isotopic variability is not discussed here. Those interested in these non-lake and non-stream data are directed to our open access database (Akers et al., 2023a).

5 Isotopic variability in lakes

The isotopic composition of a lake at a given point in time reflects its current isotope-mass balance (Gibson et al., 2016; Gonfiantini, 1986), represented as

$$V\frac{d\delta_L}{dt} + \delta_L\frac{dV}{dt} = I\delta_I - Q\delta_Q - E\delta_E \text{ (‰} \cdot m^3 \cdot year) \quad (1)$$

where V is the lake volume, t is time, I is total lake inflow, Q is total lake outflow, E is evaporation, and δ_L, δ_I, δ_Q, and δ_E are the respective isotopic compositions of the lake, inflow, outflow, and evaporation flux. Based on Eq. 1, we expect lakes with different environmental characteristics related to volume, inflow, outflow, and evaporation to exhibit spatial isotopic variability. Likewise, local weather and seasonal climate changes that affect these hydrological parameters will drive temporal lake isotopic variability. Following this understanding, we investigated which environmental parameters best explained the observed spatiotemporal variability in lake isotopes across Pituffik using our large set of lake water samples.

The full set of 67 lakes included in our isotopic dataset represents a near-comprehensive sampling of total lake variability on the Pituffik Peninsula (Figure 1). These lakes range in surface area from 1100–2000 m^2 for smaller ponds to nearly 260,000 m^2 for Lake Crescent, the largest non-proglacial lake in our set and on the peninsula. The lakes are distributed across much of the environmental gradient that follows the elevation rise from the lowest coastal lakes at 22 m a.s.l. to the highest lakes at 500 m a.s.l near a margin of the GrIS. The distance to each lake from the ocean varies between 0.07–17.8 km while the distance from the nearest margin of the GrIS varies between 0.0–16.9 km.

The isotopic compositions of Pituffik lakes vary widely across both space and time (Figure 3a, Figure 4). The highest lake δ^{18}O and δ^2H values of −4.7 ‰ and −80 ‰, respectively, were observed in the endorheic Angry Duck Lake on 26 July 2019, and this same sampling also produced the lowest observed *dxs* value of −42 ‰. In contrast, the lowest δ^{18}O and δ^2H values of −23.2 and ‰ −177 ‰, respectively, were observed in Half Snow Lake, a small lake abutting a permanent snow patch that is located in the vast boulder outwash plains fronting the GrIS south of the main lakes region. Many of the proglacial lakes near the Tuto Ice Ramp have similarly low isotopic ratios as Half Snow Lake, and one of these lakes (Ice Ramp Base Pond) returned the highest observed *dxs* value of +15 ‰ on 7 July 2018. Despite this wide overall range, most lake samples fall within a much more limited isotopic range (25–75% quantile ranges: δ^{18}O = −18.6 to −15.9‰, δ^2H = −148 to −134 ‰, *dxs* = −7 to +1 ‰).

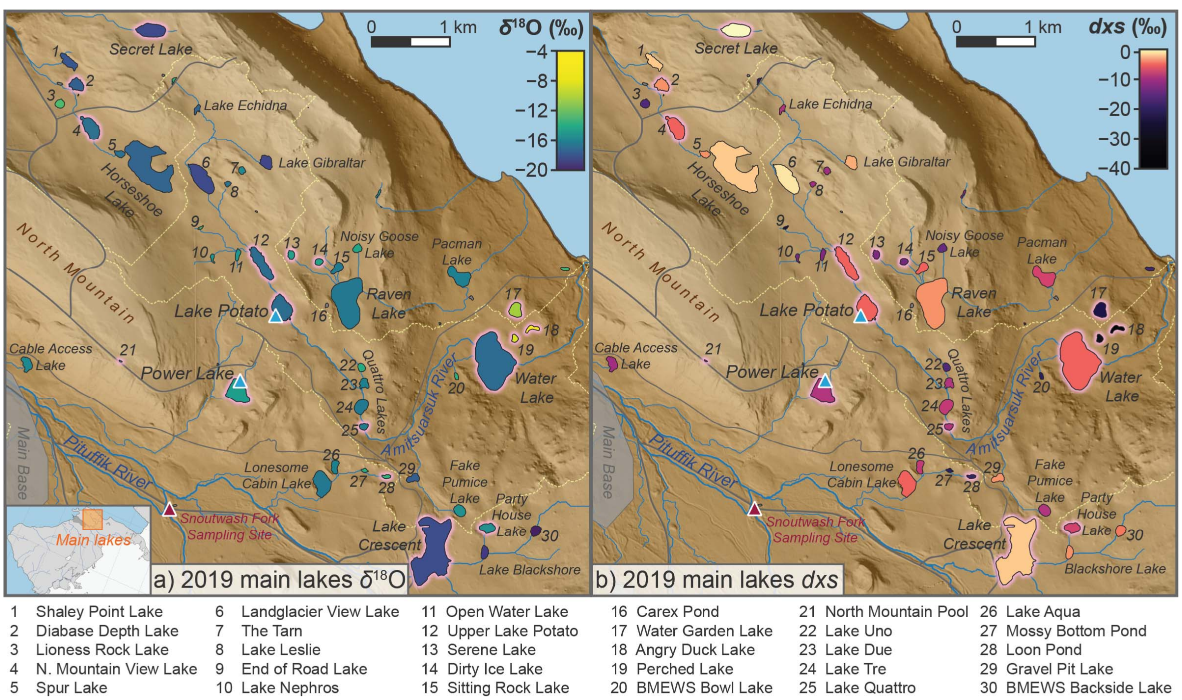

Figure 4. Water isotopic compositions of lakes sampled in mid-summer 2019 in the main Pituffik lakes region. Lakes are colored according to their measured δ^{18}O (a) and *dxs* (b) values. Although δ^2H values are not shown here, their relative spatial distribution appears

extremely similar to the $\delta^{18}O$ values (a). Broader regional context, minor icon identification, and geospatial data sources can be found in Figure 1.

5.1 Spatial variability in lake isotopic composition

5.1.1 Lake types

In order to minimize any analytical muddling from temporal isotopic evolution (L. Anderson et al., 2013; Arp et al., 2015; Cluett & Thomas, 2020; Gibson & Reid, 2014), we focused our spatial analysis of lake isotopic composition on water samples from 63 lakes that were collected in the two-week mid-summer 2019 sampling period. These 63 lakes were classified by lake type into 26 headwater, 17 downstream, 4 endorheic, 6 vale, 5 proglacial, and 5 altered lakes. The isotopic compositions of the different lake types during this period are generally well-grouped and distinct from each other (Figure 5a). The endorheic lakes are the most distinct with $\delta^{18}O$ and $\delta^{2}H$ values much higher than all other lakes and *dxs* values as low or lower than all other lakes. At the other extreme from the endorheic lakes, proglacial lakes have *dxs* values higher than all other lakes as well as some of the lowest $\delta^{18}O$ and $\delta^{2}H$ values. Headwater and downstream lakes have intermediate isotopic values, although the isotopic range for headwater lakes is much larger and completely overlaps the range in downstream lakes, which can be expected as every downstream lake is connected to at least one headwater lake. Additionally, headwater lakes as a whole have higher mean $\delta^{18}O$ and $\delta^{2}H$ values and lower mean *dxs* values than downstream lakes. Vale lakes bridge the isotopic value gap between headwater/downstream lakes and proglacial lakes, and altered lake isotopic compositions are similar to headwater and downstream lakes. Although this isotopic similarity suggests that human disruptions have not dramatically changed the hydrology of the altered lakes from what might be naturally expected, we exclude these lakes from subsequent analyses out of caution.

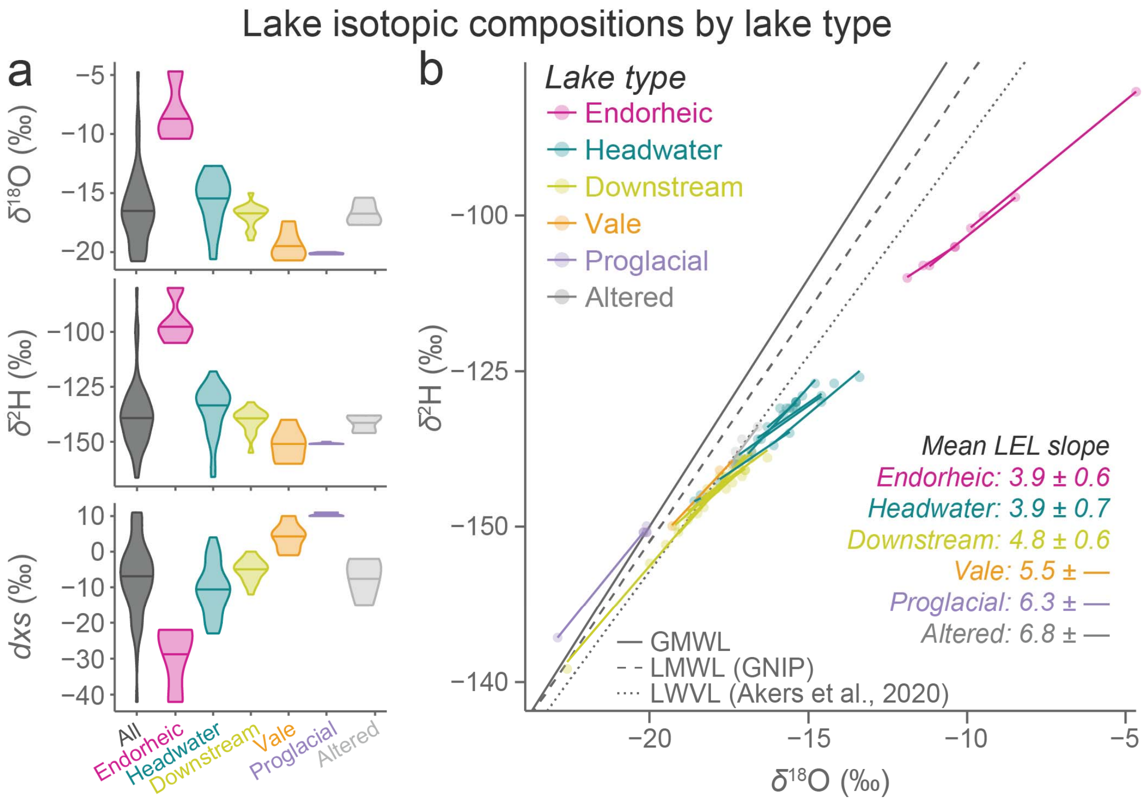

Figure 5. Isotopic composition of lakes sampled across Pituffik grouped by lake type category. In (a), violin plots show the isotopic composition distribution of all lakes sampled in 2019 (black) as well as split by lake type (colored). Data are plotted so that the maximum width is equivalent between groups, regardless of sample count. Within each violin, the median value per group is shown by a solid horizontal line. In (b), δ^2H vs. δ^{18}O is plotted to show local evaporation lines (LELs) for every lake that was sampled at least three times across 2018 and 2019. Each LEL represents a single lake or pool, and the LELs are colored according to lake type. The mean and 95% confidence interval of LEL slope values are displayed per lake type at lower right. Note that the vale and altered lake slopes have no confidence interval as there is only one lake per type that was sampled at least three times. Note also that the proglacial lakes do not display a true LEL as the values do not fall below the LMWL in δ^{18}O–δ^2H space. The global meteoric water line (GMWL, solid gray), local meteoric water line (LMWL, dashed gray) based on GNIP data (IAEA/WMO, 2022), and local water vapor line (LWVL, dotted gray) (Akers et al., 2020) are shown for reference.

The LELs of individual lakes suggest that evaporation is a key driver of the isotopic differences between lake types (Figure 5b). Examining lakes that were sampled at least three times across 2018 and 2019 (number of lakes per type: endorheic = 3, headwater = 7, downstream = 3, vale = 1, proglacial = 2, altered = 1), we observe that lakes and lake types with isotopically heavier waters have LELs with lower slopes. This observation suggests that these isotopically heavier lakes exist in more arid environments that promote lake water evaporation. This dominance of evaporation agrees with isotopic results from lake systems elsewhere in Greenland (Kopec et al., 2018; Leng & Anderson, 2003) and in boreal Canada (Gibson, 2002; Gibson & Reid, 2014) and is notably greater than reported for subarctic lakes in Sweden (Jonsson et al., 2009).

The mean lake LEL slope value differs depending on the method of calculation, and this difference is important when comparing LEL slopes across studies. The LEL slope calculated from combining all the lake data, as reported in many other relevant studies (Gibson & Edwards, 2002; Kopec et al., 2018; Leng & Anderson, 2003; Stansell et al., 2017), is 5.1±0.1. This slope is lower than reported for coastal lakes in central West Greenland and Arctic Alaska (Leng & Anderson, 2003; MacDonald et al., 2017) but higher than more inland lakes in central West Greenland and the Canadian Arctic (Gibson & Edwards, 2002; Kopec et al., 2018; Leng & Anderson, 2003). The intermediate slope values for Pituffik suggest that the arid High Arctic summer coupled with the proximity to the GrIS and its drying katabatic winds promote a more evaporative environment than might be expected for its coastal location. However, if the LELs are calculated individually for lakes and then averaged, the mean slope value is 4.6±0.5. Few Arctic studies report lake LELs based on this method for comparison, but our observed slope difference highlights the flawed assumption of identical initial water isotopic compositions made when aggregating all regional lakes into a single LEL (Bowen et al., 2018; MacDonald et al., 2017).

Indeed, the intersections between individual Pituffik lake LELs and the LMWL suggest that the initial isotopic composition of lakes differs by lake type. The sampled proglacial lakes do not produce an LEL, suggesting that their waters have not experienced substantial evaporative loss and that their observed isotopic composition is their initial isotopic composition. This is logical as the proglacial lakes are directly in contact with and supplied by the melting of the GrIS. For the other lake types, the mean predicted initial isotopic composition is the heaviest for endorheic lakes ($\delta^{18}O = -17.1\pm0.9$ ‰, $\delta^{2}H = -131\pm7$ ‰) followed by headwater lakes ($\delta^{18}O = -19.7\pm0.8$ ‰, $\delta^{2}H = -150\pm6$ ‰), downstream lakes ($\delta^{18}O = -20.9\pm0.8$ ‰, $\delta^{2}H = -159\pm6$ ‰), and then vale lakes ($\delta^{18}O = -20.6$ ‰, $\delta^{2}H = -157$

‰, based on single LEL). The isotopically heavier initial values predicted for endorheic and headwater lakes suggest that these lakes are sourcing relatively more warm season precipitation versus isotopically light winter snowpack, perhaps due to their smaller and more isolated watersheds that limits their supply from tundra-wide snowpack melt.

Hierarchical clustering based on the lake water δ^{18}O and *dxs* values (Figure 6a–b) sorts the lakes in four main clades and supports our lake type categorization as reflecting real differences in lake hydrology. Although the lake types are not perfectly sorted into the clades, the clades resulting from the hierarchical clustering are better explained by lake type category than by specific lake parameters such as size, elevation, or particular watershed. This argues that lake isotopic composition is strongly influenced by hydrological connectivity, which is central to lake type character and categorization.

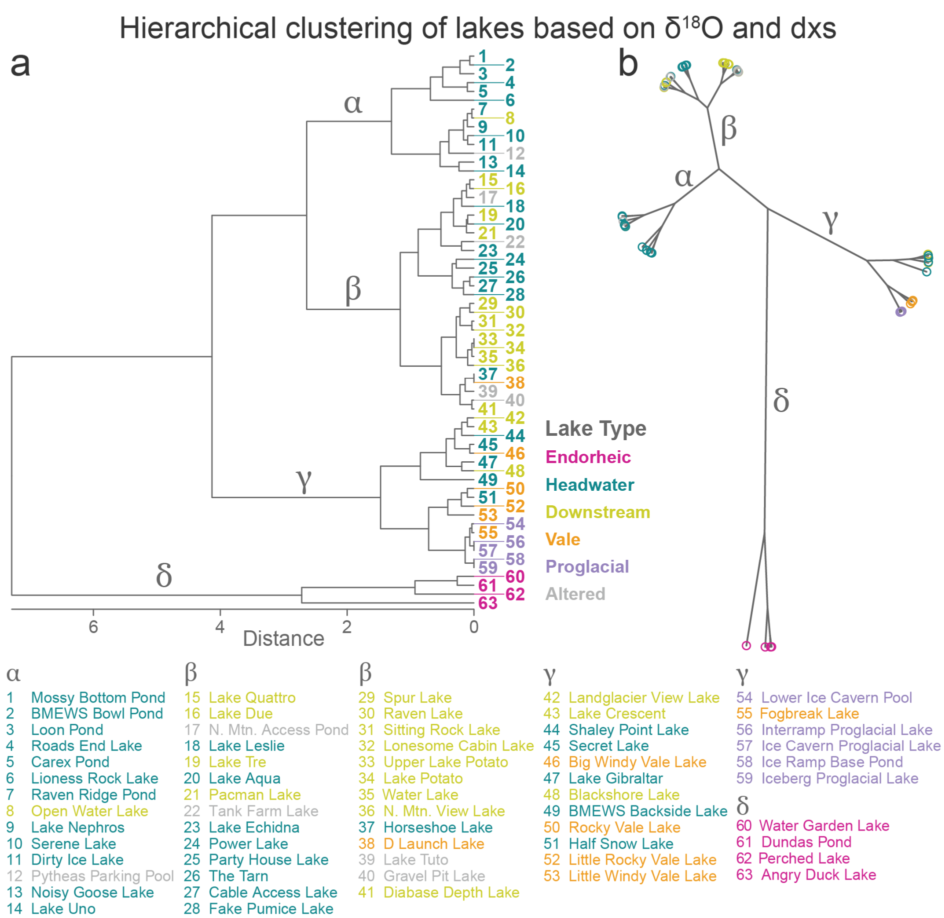

Figure 6. Hierarchal clustering results for Pituffik lakes based on δ^{18}O and *dxs* values. Results are shown in two forms of dendrogram (a, b) with individual lakes colored according

to lake type. Four prominent clades are identified with Greek letters. Lake names referencing the numerical results in (b) are provided at bottom.

The four endorheic lakes comprise their own clade (δ) well-separated from all other lakes, validating the isotopic distinctiveness of this lake type. The extreme isotopic values and distinct clade identity of the endorheic lakes reflect evaporation's dominance of their water balance as supported by their shared lowest mean LEL slope values (Figure 5b). Angry Duck Lake, the lake whose 2019 water sample had the heaviest isotopic composition and lowest *dxs* values of all lake samples, is a very shallow endorheic lake whose size changes year to year reflecting water balance. In fact, many of the Pituffik endorheic lakes have severely shrunk in size or even disappeared since 2020. Similarly low endorheic lake levels observed in 2016 (Copernicus, 2019) and 1949 (Figure S6) suggest that the loss of these endorheic lakes is not a recent phenomenon due to climate change, but rather that they are simply highly sensitive to short-term water balance changes. These endorheic lakes function similarly to idealized evaporation pans due to their lack of channel outflow, permafrost that blocks groundwater inflow and outflow, and small, self-contained basins that limit input from precipitation. The low mean LEL slope value and isotopically heavy initial water values for endorheic lakes (Figure 5b) reflect a consistently arid environment whose lake waters are perhaps more sensitive to and reflective of isotopically heavier summer precipitation.

Headwater and downstream lakes have similar isotopic values, but the LELs and cluster analysis support that they have detectable hydrological differences. The lower LEL slope values, higher mean $\delta^{18}O$ and $\delta^{2}H$ values, and lower mean *dxs* values of headwater lakes suggests that they have on average greater evaporation losses than downstream lakes (Figure 5a–b). This may seem counterintuitive at first because downstream lakes receive water that has already experienced isotopic change from evaporation in upstream lakes, and additional evaporation in a downstream lake should only add to the existing isotopic changes. However, headwater lakes have a smaller surface area on average than downstream lakes (mean ± 95% confidence interval: 20950±16230 m^2 vs. 65290±38560 m^2, respectively), and heavier isotope enrichment in smaller lakes due to greater relative evaporation loss has been previously reported for Greenlandic lakes (Kopec et al., 2018). Assuming that surface area is correlated with volume, the smaller volume of headwater lakes would enhance the relative evaporation component of the headwater lake water balance, and their smaller watersheds also limit the amount of precipitation input from runoff. Many of the smaller headwater lakes are shallow enough to freeze to their beds in winter, resulting in earlier spring ice melt and greater potential summer evaporative loss (Arp et al., 2015). Additionally, these headwater lakes likely only supply a minor component of the overall water input to downstream lakes relative to total basin runoff, and thus their evaporation-altered water does not likely not provide substantial input by volume to downstream lakes.

Indeed, one clade identified in the cluster analysis (α) almost entirely contains headwater lakes, and closer investigation of this clade's lakes reveals that they are all particularly small lakes (surface area mean ± 95% CI = 5750±1630 m^2) without stream channel connections to their larger watersheds. Clear downstream drainage does occur from these lakes, but their drainage routes and shores are thickly vegetated in moss which slows outflow and hydrologically isolates the lakes. The largest clade (β) contains a mix of headwater and downstream lakes that are generally larger in surface area and better hydrologically connected than the α-clade. Notably, nearly half of all downstream lakes are exclusively clustered in a single subgroup of this clade despite belonging to four different watersheds, suggesting that their downstream nature is a stronger determinant of isotopic composition than their particular hydrologic basin.

Finally, the remaining clade (γ) initially appears to be a confusing mix of headwater, downstream, vale, and proglacial lakes. However, these lakes mostly share a rocky rather than vegetated shore and a direct hydrologic connection to ice and snow patches that linger long past the early summer melt of the general tundra snowpack. The proglacial lakes comprise one distinct subgroup of this clade along with a vale lake (Fogbreak Lake) that is hydrologically similar to a proglacial lake as it has only recently formed as a large permanent snow patch partially retreated. Proglacial and vale lakes have isotopic values very similar to the mean value of Pituffik snow and ice samples (Figure 3) which reflects their summer-long recharge from the melting of permanent snow from the GrIS or patches shaded by the steep vale valley slopes.

The headwater and downstream lakes in the γ-clade generally have watersheds that drain substantial high altitude areas, and the continuing late season snowmelt supply pushes the isotopic character of these lakes closer to proglacial and vale lakes. For example, Half Snow Lake is classified as a headwater lake based on its hydrological setting, but it provided the isotopically lightest lake water sample in our dataset and falls within the γ clade. As its name suggests, Half Snow Lake abuts a large permanent snow patch, and this snow patch provides a steady supply of isotopically light meltwater to Half Snow Lake over the summer in a manner hydrologically similar to the proglacial lakes. Overall, it is important to note that while each lake type can be said to have a typical isotopic and environmental character, the lake type categories do not have hard boundaries, and several lakes are clearly hybrid or transitional lake types. Additionally, hydrological factors specific to each lake other than the simple lake type category (e.g., presence of local snow patches, depth and thermal stratification, etc.) can skew individual lakes away from what would be expected based solely on the mean isotopic values of their lake type.

5.1.2 Hydrological parameters

Lake type sets the general value expected in a lake's isotopic composition, but other environmental parameters influence the isotopic composition of Pituffik lakes within each lake type group. To examine these parameters, we performed multiple regression and LASSO regressions on the subset of 42 headwater and downstream lakes sampled in mid-summer 2019 from the main lakes region (Figure 1b, Figure 4). Both multiple and LASSO regressions identified elevation, surface area, and watershed area as having important influences on lake isotopic composition, but their relative importance differed depending on specific isotopic variable (Figure 7, Table S2). Both lake surface area and watershed area are known as key components of lake water balance in the Arctic (e.g., Gibson & Reid, 2014; Wilcox et al., 2023), and it is thus not surprising that they emerged as strong environmental drivers at Pituffik. Day of year sampled and the distances from the GrIS and ocean did not have notable relationships with isotopes. This is in contrast to prior studies in Søndre Strømfjord, Greenland (Kopec et al., 2018; Leng & Anderson, 2003), and northern Scandinavia (Kjellman et al., 2022) that detected clear relationships between lake isotopic composition and distance from the ocean. However, both these studies examined lakes on much longer transects away from the coast (150–460 km) than available at Pituffik (<20 km), and it is probable that the distance from the ocean simply is not large enough at Pituffik to emerge as a primary driver of isotopic variability.

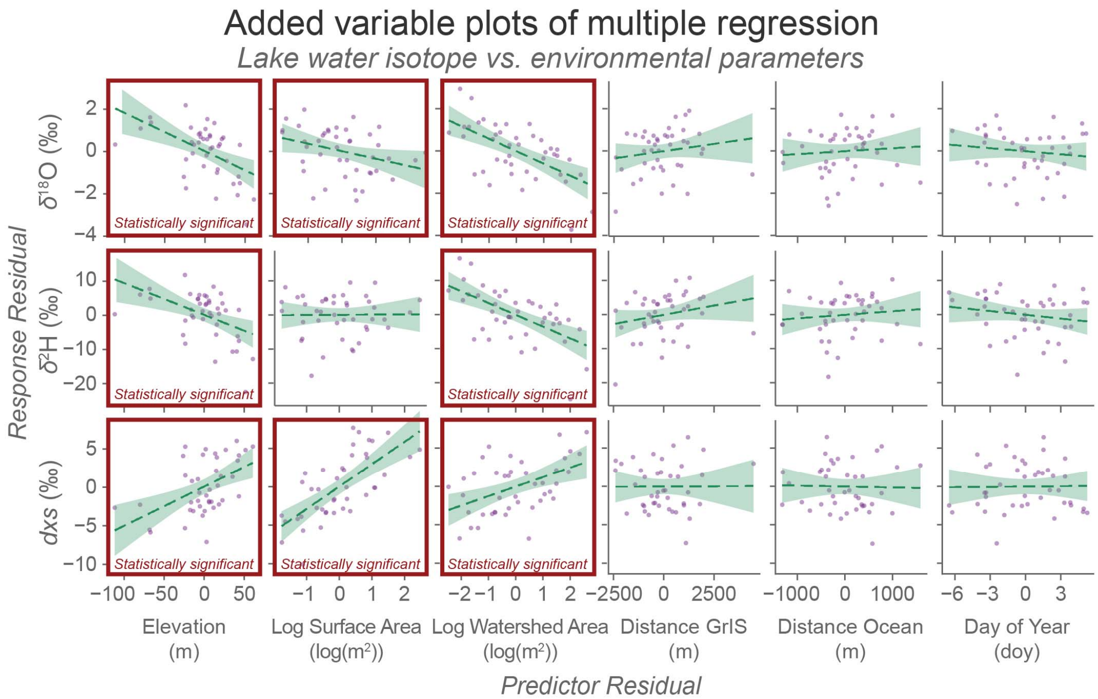

Figure 7. Added variable (i.e., partial regression) plots of the multiple regression of each lake isotopic variable versus six environmental parameters. Regressions are shown as green dashed lines with 95% confidence intervals of the regression shown in green shading. Lake samples included in the multiple regressions were restricted to headwater and downstream lakes sampled in mid-summer 2019 from the main lakes region north of the air base. Parameters that produced statistically significant multiple regression coefficients for specific isotopic variables (Table S2) are outlined by red boxes.

The $\delta^{18}O$ and $\delta^{2}H$ share similar influential parameters on lake isotopic composition (Figure 7, Table S2). For $\delta^{18}O$, the most influential parameter is the lake watershed area followed by elevation and then lake surface area. For $\delta^{2}H$, LASSO regression identified lake watershed area as the sole important parameter, but we also included elevation in the multiple regression as its inclusion substantially improved the regression strength. The sensitivity of $\delta^{18}O$ and $\delta^{2}H$ to lake watershed area probably reflects the degree of precipitation recharge the lake is receiving relative to the lake total volume (assuming that the lakes with larger surface areas generally have larger volumes). Since precipitation and the snowpack are isotopically lighter than average lake values (Figure 3a), lakes with larger watersheds will logically have greater precipitation input and thus lower $\delta^{18}O$ and $\delta^{2}H$ values. Lakes having lower $\delta^{18}O$ and $\delta^{2}H$ values with higher elevation is likely a product of the altitude effect (Dansgaard, 1964;

Rozanski et al., 1993), and may also reflect reduced evaporation at higher elevations as suggested by the *dxs* results. The weak relationship observed where lakes with larger surface areas are isotopically lighter is potentially because these lakes with larger surface areas tend to have larger volumes, and the larger volumes of these lakes are more buffered against the heavy isotope enrichment impact of evaporation. However, this weak relationship may also party arise from the positive correlation between lake surface area and watershed area (r = 0.57) since headwater lakes with smaller watersheds tend to be smaller in surface area.

In contrast, *dxs* is most influenced by lake surface area, followed by elevation, and finally lake watershed area (Figure 7, Table S2). This strong influence of lake surface area on *dxs* reflects the sensitivity of small lakes to evaporation-driven isotopic effects (Kopec et al., 2018). Most of the smaller headwater and downstream lakes are shallow, and as a result, these lakes' isotopic compositions can change relatively quickly under strong evaporative conditions. As previously stated, these smaller lakes likely freeze to their beds in winter, and these "bedfast ice" lakes melt out earlier and have longer seasonal exposure to evaporation than larger lakes that have floating ice (Arp et al., 2015). Thus, the smaller lakes generally greater evaporative water loss and lower *dxs* values. Lakes at higher elevations have higher *dxs* values, suggesting that they have less evaporative impacts. This is most likely due to the slightly lower temperatures at higher elevations that reduce direct evaporation and extend the period of lake ice cover when no evaporation can occur. Additionally, the tundra snowpack lasts longer at higher altitudes, and higher lakes will receive the high *dxs* runoff from this snowpack for a longer portion of the summer. Finally, lakes with larger watersheds have higher *dxs* values, which reflects how larger watersheds provide a greater volume of high *dxs* precipitation and snow melt input relative to lake volume compared to lakes in smaller watersheds.

5.2 Temporal variability in lake isotopes

5.2.1 Lake isotopic variability over summer 2018

Over summer 2018, we observe consistent isotopic changes across the multi-annual subset of 18 Pituffik lakes and 2 pools (simplified hereafter to just "20 lakes") studied for temporal evolution (Figure 8a). Nearly all these lakes are isotopically heavier (19 of 20 lakes, exception: Angry Duck Lake) with lower *dxs* values (18 of 20 lakes, exceptions: Angry Duck Lake and Lake Tuto) at the end of summer than in early summer. This change is consistent with observations in other high latitude lakes where lake waters are isotopically lighter in spring and early summer due to snowpack melt inflow but become enriched in heavier isotopes by late summer due to evaporation losses (Gibson & Reid, 2014; Leng & Anderson, 2003). The two lakes that did not follow this isotopic evolution can be explained by their particular lake environments: Angry Duck Lake is a very shallow endorheic lake whose isotopic composition is likely very sensitive to recent precipitation events while Lake Tuto is a large, high altitude lake less sensitive to evaporation and fed by melting snowpack well into the late summer. Although spatially, lakes with smaller surface areas are isotopically heavier with lower *dxs* values (Figure 7), lake surface area does not have a clear impact on the rate and magnitude of isotopic change over summer 2018 (Figure 8a).

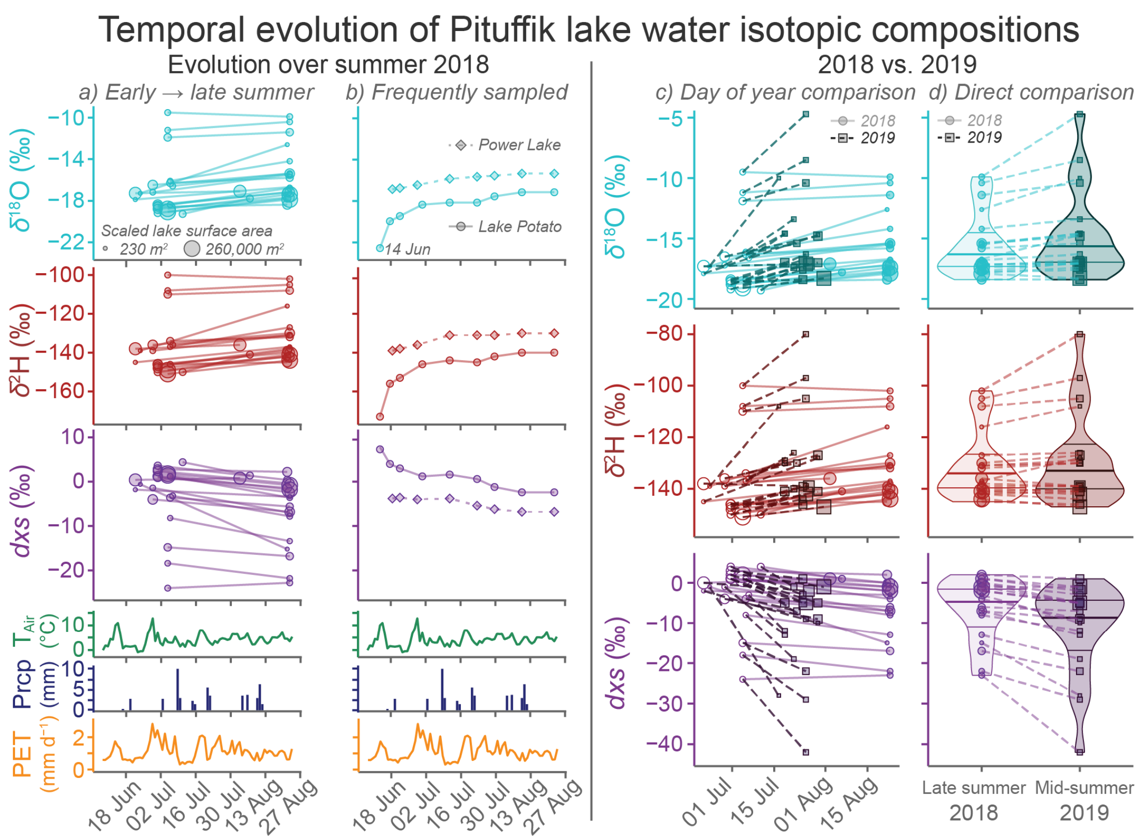

Figure 8. Water isotopic composition changes in select Pituffik lakes over summers 2018 and 2019. Lakes included here are part of the multi-annual subset of 18 lakes and 2 pools that were sampled during each of the three main sampling periods. The size of each point represents the relative log-scaled surface area of the lakes, which was identified as a primary factor in evaporation's impact on isotopic composition. In (a), isotopic differences in the lakes from early to late 2018 summer are shown while (b) shows the isotopic changes over

summer 2018 for the frequently sampled Power Lake (diamonds, dashed line)and Lake Potato (circles, solid line). Daily mean air temperature, precipitation amount, and potential evapotranspiration over summer 2018 are shown at the bottom of (a) and (b) for environmental context (Muscari, 2018; Singer et al., 2021; USAF, 2019). For (c) and (d), interannual water isotopic differences between summer 2018 (circles) and summer 2019 (squares) are shown. In (c), isotopic values are plotted by sampling day of year. Lines connect early summer 2018 values to late summer 2018 values (solid lines) and to mid-summer 2019 (dashed lines) values for each individual lake and pool. In (d), isotopic values are directly compared between late summer 2018 and mid-summer 2019 samples with overall value distributions illustrated with violin plots. The isotopic values for each individual lake and pool are connected by dashed lines.

The frequent sampling performed at Lake Potato and Power Lake grant us further insight into summer lake isotopic evolution and into how short-term weather events influence isotopic variability. Over summer 2018, both Lake Potato and Power Lake share increasing δ^{18}O and δ^{2}H values and decreasing *dxs* values (Figure 8b). Both lakes have similar LEL slopes (Lake Potato: 6.1 ± 0.3; Power Lake: 6.0 ± 0.9), and the intersections of these LEL with the LMWL estimate that the initial water isotopic compositions for Lake Potato is δ^{18}O = −22.9 ‰ and δ^{2}H = −174 ‰ and for Power Lake is δ^{18}O = −23.2 ‰ and δ^{2}H = −176 ‰. These values are very close to the annual amount-weighted GNIP precipitation mean values of −22.5 ‰ and −173 ‰. The excellent agreement between the three isotopic compositions (Lake Potato initial water, Power Lake initial water, mean annual precipitation) gives credence to the improved accuracy obtained when restricting LELs to individual water bodies rather than regional aggregates and supports the close approximation of permafrost-bound tundra lakes to the evaporation pan model that the technique is founded upon (Bowen et al., 2018; Gibson et al., 1999).

Although only collected at Lake Potato, the first lake water sample taken on 14 June 2018 highlights the rapidly changing Pituffik hydrology during the early summer thaw. This sample has the second lowest δ^{18}O and δ^{2}H values of any lake water sample in our database, but the δ^{18}O and δ^{2}H values of the next sample taken only four days later increased by 2.6 ‰ and 17 ‰, respectively. This four-day rise is the same magnitude of isotopic change then observed over the next two months in Lake Potato from 18 June to 23 August. This extreme isotopic change is largely explained by the different thaw timings of the tundra snowpack and the Lake Potato ice cover. On 14 June, warm and sunny conditions led to extensive snowpack melt across the tundra, but Lake Potato itself maintained a nearly intact ice cover that greatly limited mixing between the inflowing snow melt and the pre-existing lake water in and beneath the ice. Water samples taken directly of the snowpack meltwater on this day had similarly low isotopic values as the Lake Potato sample, and our sample of the near surface water, therefore, simply captured mostly isotopically light snowpack melt flowing over the isotopically heavier lake ice. By 18 June, the lake ice had more fully retreated, and the heavier δ^{18}O and δ^{2}H values of this date's sample reflect the mixing in of the pre-existing lake waters. In further support, the Lake Potato *dxs* values drop from a relatively high +8 ‰ on 14 June (suggesting a source with limited past evaporation, such as snow melt) to +4 ‰ on 18 Jun (suggesting the mixing in of waters with greater past evaporation, such as lake water).

Although the LEL slopes are similar between the Lake Potato and Power Lake, the lakes' isotopic compositions evolve differently in early summer based on their upstream drainage sizes and ice coverage. Lake Potato displays a strong early season thaw pulse and recovery from 18 June to 01 July 2018 when the isotopically light waters supplied by snowmelt become steadily heavier while *dxs* values decrease. This thaw pulse recovery follows the decreasing input of snowpack meltwater once the local snowpack disappears and the continuing melt and reincorporation of the lake's isotopically heavier ice and last season's deeper waters (Figure S5). In addition to the mixing in of older lake waters which carry lower *dxs* values from prior summer evaporation, new evaporation might also occur and further decrease lake *dxs* values as Lake Potato's ice cover retreated. In contrast, Power Lake has a much less dramatic thaw pulse and recover, which is likely due to its much smaller drainage basin (sixteen times smaller than Lake Potato) which receives snowpack meltwater only from the small region directly surrounding the lake. Additionally, the *dxs* values observed from 18 June to 12 July in Power Lake are very stable and likely resulted from the near-continuous ice cover the lake held well into mid-July (Figure S5) which prevented any new evaporation from substantially altering the lake water isotopic composition.

The two lakes also show different responses to precipitation events that occurred in July. Nearly all ice in Lake Potato was melted by 04 July 2018 (Figure S5), and the isotopic values then change very little for the rest of the month. With the lack of ice cover, we would expect to observe some evaporative enrichment of heavy water isotopes under relatively high PET, but the June trend of increasing $\delta^{18}O$ and $\delta^{2}H$ values and decreasing *dxs* values at Lake Potato is interrupted in July by a plateauing of values less strongly observed in Power Lake (Figure 8b). This plateauing may be due to a series of July rain events whose isotopic values (mean $\delta^{18}O$: −19.1 ‰; $\delta^{2}H$: −150 ‰; *dxs*: +2.6 ‰) would serve to counteract any effect from evaporation. With the much larger drainage basin of Lake Potato, the runoff from any precipitation event would have a more magnified effect on Lake Potato water isotopes compared to Power Lake.

Evaporative enrichment in heavier isotopes is evident in both lakes from late July through mid-August. Under drier and warmer conditions with greater PET than early July, the $\delta^{18}O$ values of both lakes increase at the same time that *dxs* values decrease (Figure 8b). Unusually, Power Lake's $\delta^{2}H$ values barely change from 12 July through the end of summer despite its $\delta^{18}O$ values increasing until 10 August. This possibly reflects a situation where the limited rainfall runoff that Power Lake received was isotopically balanced with regards to $\delta^{2}H$ with evaporative loss that preferentially removes water with lighter hydrogen isotopes, but we lack the ability to verify this conjecture. Finally, both lakes exhibit almost no isotopic change between 10 August and the last observation on 23 August as daily mean temperatures were rapidly dropping to near freezing, and evaporation was much more limited.

For broader applications, the isotopic observations from these two lakes can be used to estimate how much temporal isotopic change might occur on short timescales, such as within each of the 15–20 day long periods where we sampled our multi-annual 20 lakes subset. Based on observed changes in 2018 at Lake Potato and Power Lake (Table S3), a lake sampled at the beginning and end of a 20-day sampling period could see, on average, a $\delta^{18}O$ increase of 0.4 to 1.2 ‰, a $\delta^{2}H$ increase of 3.2 to 6.4 ‰, and a *dxs* decrease of 0.8 to 2.4 ‰. Changes toward the beginning of summer might be twice these values while changes toward the end of summer would more likely be near zero. We can consider these values to represent a rough upper bound on the potential degree of temporal isotopic variability within a 20-day sampling period, but we also note that most of our 20 lakes were sampled together with less than a week's separation and thus have a limited potential impact from temporal isotopic evolution.

5.2.2 Interannual summer lake isotopic values in 2018 versus 2019

Our 2019 lake sampling took place over the last two weeks in July, and we use the isotopic composition of these samples relative to those taken in 2018 to gain insight into how lake water isotopes may change from year to year. However, because the timing of the 2019 sampling falls between the two sampling periods in 2018, we cannot directly compare values between the years because the lake isotopic composition is constantly evolving over the summer. Based on observations at Potato Lake and Power Lake (Figure 8b), we assume that $\delta^{18}O$ and $\delta^{2}H$ values in Pituffik lakes generally increase and *dxs* values decrease from the time of early season snowpack melt in late May/early June until the middle of August. Thus, the isotopic values of the lakes in middle to late August should be their maximum $\delta^{18}O$ and $\delta^{2}H$ and minimum *dxs* values, with the degree of isotopic change over the summer primarily reflecting the amount of evaporative water loss.

Overall, the isotopic values of our lake dataset suggest that more evaporation occurred in 2019 than in 2018. By late July 2019, 95% of the lakes in the multi-annual subset already had lower *dxs* values than the values measured in late August 2018, signifying greater evaporative loss. Similarly, 85% and 65% of lakes had higher $\delta^{18}O$ and $\delta^{2}H$ values indicative of greater evaporation, respectively, in late July 2019 than late August 2018 (Figure 8c–d), which is expected as evaporation also enriches remaining water in heavier isotopes. For many lakes, the differences in *dxs* values between the two years were extremely large: five lakes had *dxs* values > 7 ‰ lower in 2019 than in 2018 with the largest difference of 20 ‰ lower *dxs* observed in an isolated roadside pool. Additionally, the LEL calculated from these 18 lakes and 2 pools in mid-summer 2019 had a lower slope value (4.9±0.2) than either early or late summer 2018 (5.3±0.2 and 5.1±0.2, respectively), also suggesting a more arid environment existed in 2019 than in 2018 (Figure S8). All together, these values suggest that substantially more evaporative water loss had occurred across Pituffik lakes by the end of July in 2019 than during the entire summer of 2018.

Weather differences between the summers 2018 and 2019 support conditions being more favorable for evaporation in 2019 as we inferred from the lake isotopic compositions. Weather conditions and surface melt extent in summer 2018 were close to 1981–2010 averages (Mote, 2020; USAF, 2019), but summer 2019 was one of the warmest and sunniest seasons on record for Greenland with massive volumes of surface ice melted from the GrIS across the island (Sasgen et al., 2020; Tedesco & Fettweis, 2020). Although the 2019 GrIS melt peaked with an extraordinary event at the end of July, the entire summer had remarkedly stable anticyclonic conditions and above average surface melt (Mote, 2020; Tedesco & Fettweis, 2020).

At Pituffik, the persistent anticyclonic conditions during June–August 2019 resulted in that summer being 4.5°C warmer and having an atmospheric pressure 12 hPa higher than the same period in 2018 (Muscari, 2018). Summer 2019 was also drier than summer 2018, both in total precipitation (32 vs. 54 mm, respectively) and in mean relative humidity (68% vs. 79%, respectively) (Muscari, 2018; USAF, 2019). When totaled over each summer, modeled daily PET (Singer et al., 2021) for Pituffik was almost two times greater in 2019 than 2018 (177 mm vs. 96 mm, respectively). Indices for the North Atlantic Oscillation and Arctic Oscillation show that atmospheric circulations were very different between the two years, with consistent positive indices in 2018 and consistent negative indices in 2019. A negative North Atlantic Oscillation is associated with greater evaporation of Pituffik surface waters due to the local foehn-like conditions as southerly winds are forced over the GrIS and Tuto ice dome (Akers et al., 2020). The enhanced pressure gradients of the negative North Atlantic Oscillation also drive stronger katabatic winds that also increase evaporative potential (Kopec et al., 2018). Finally, the consistently warmer conditions in 2019 brought much earlier ice-free conditions to the Pituffik lakes that lengthened the evaporation exposure period, with ice coverage in July 2019 running 16–20 days ahead of conditions in 2018 (Copernicus, 2019).

Other than evaporation, interannual lake isotopic variability has also been suggested to reflect isotopic differences in the winter snowpack resulting from varying winter storm sources and air temperature (Kjellman et al., 2022). Although we do not have early summer water samples from 2019 to directly compare the isotopic composition of tundra snowpack meltwater with our samples from 2018, we do not believe that snowpack isotopic variability best explains the observed interannual differences in Pituffik lake isotopic composition. This would require the 2018–2019 winter snowpack to have been isotopically heavier than the 2017–2018 snowpack. This seems unlikely for Pituffik because the winter 2018–2019 had a colder mean air temperature and synoptic conditions which would suggest that the snowpack melting in spring 2019 would more likely have lower δ^{18}O and δ^{2}H values than the 2018 spring snowpack (Akers et al., 2020). More precipitation was reported in the seven months leading to June 2018 than June 2019 (53.4 vs. 29.6 mm water equivalent), possibly resulting in a greater tundra snowpack water volume in 2018. Greater snowpack volume could have possibly flushed the lakes with more snowmelt in 2018 than 2019 leading to isotopically lighter lakes in 2018, but limits imposed by lake ice coverage and snow melt bypass (Wilcox et al., 2022) likely dampen the impact of different snowpack volumes. Overall, the sheer magnitude of isotopic change between 2018 and 2019, the exceptionally negative *dxs* values in 2019, and the lower lake LEL slope in 2019 strongly support our conclusion that the isotopic differences between the 2018 and 2019 are primarily due to differences in summer weather that affected evaporation rather than different snowpack isotopic compositions.

6 Isotopic variability in streams

The stream sites we sampled across the Pituffik region have less isotopic variability than lakes (Figure 3a), but their isotopic differences can still be linked to the environmental character of their watersheds. We find that the isotopic composition of a stream is most clearly determined by the relative contribution of runoff from tundra snowpack melt versus GrIS glacial melt, with a smaller influence also from rain events and lake water evaporation in particular streams. The winter snowpack across the Pituffik tundra has distinctively low δ^{18}O and δ^{2}H values due to its condensation at very low temperatures and a substantial rain out effect during the moisture transit to northwest Greenland over sea ice and/or over the GrIS (Akers et al., 2020; Dansgaard, 1964; Rozanski et al., 1993).

In contrast, δ^{18}O and δ^{2}H values of glacial ice from the Tuto dome and its direct meltwater runoff (Akers et al., 2023a; Csank et al., 2019; Reeh et al., 1990) (δ^{18}O ≈ −18 to −21 ‰, δ^{2}H ≈ −138 to −156 ‰) are generally higher than the isotopic values that we observed in the winter tundra snowpack (δ^{18}O ≈ −20 to −39 ‰, δ^{2}H ≈ −138 to −300 ‰) and in the runoff of this tundra snowpack in early summer (δ^{18}O ≈ −21 to −23 ‰, δ^{2}H ≈ −155 to −174 ‰). Although meltwater coming off the GrIS might be expected to be isotopically light due to the high elevation and coldness of the ice dome, the higher GrIS isotopic values may result from the fact that summer precipitation that falls as rain on the tundra will often fall as snow on the GrIS. This summer snow can draw upon local moisture with relatively high δ^{18}O and δ^{2}H values from ice-free Baffin Bay (Akers et al., 2020). As a result, this seasonal difference in snow origin allows us to distinguish between water sourced from tundra snowpack versus the GrIS. While the snowpack on the tundra will be almost entirely biased toward low δ^{18}O and δ^{2}H from winter snowfall, the ice of the nearby GrIS will have higher mean isotopic values due to the inclusion of snow that has fallen all throughout the year, including summer.

In contrast to the lake studies, *dxs* has much more limited value in stream isotopic interpretation as *dxs* values do not consistently differ between most stream water sources such as the tundra snowpack and GrIS. Evaporation of source waters occurs very little for streams primarily sourced by meltwater, but streams with significant lake water components can be identified by their low *dxs* values. Summer rain on the tundra has relatively high δ^{18}O and δ^{2}H values values and low *dxs* values (Figure 3a), but the small volume and intermittent occurrence of rain events limit their impact in comparison to snowpack and GrIS melt for most streams.

6.1 Spatial variability in stream isotopes

Generally, spatial variability in stream isotopic composition is much more limited that the variability observed in lakes across Pituffik. Focusing on three stream networks that we repeatedly sampled (Pituffik River, Sioraq River, Amitsuarsuk River), we note that all six frequently sampled Pituffik and Sioraq River sites have broadly similar isotopic values while samples from the Amitsuarsuk River have much higher δ^{18}O and δ^{2}H values and lower *dxs* values (Figure 9a). These isotopic values suggest that while evaporation does not substantially affect the source waters supplying any site along the Pituffik or Sioraq Rivers, it has clearly altered the source waters supplying the Amitsuarsuk River. The δ^{18}O vs. δ^{2}H linear regressions of the streams (i.e., their local water lines, or LWLs) (Figure 9b) support this conclusion as the Pituffik and Sioraq River LWLs do not deviate from the LMWL but the Amitsuarsuk River LWL forms a distinct LEL with a slope value (5.0±0.5) much lower than the LMWL slope (7.5±0.4).

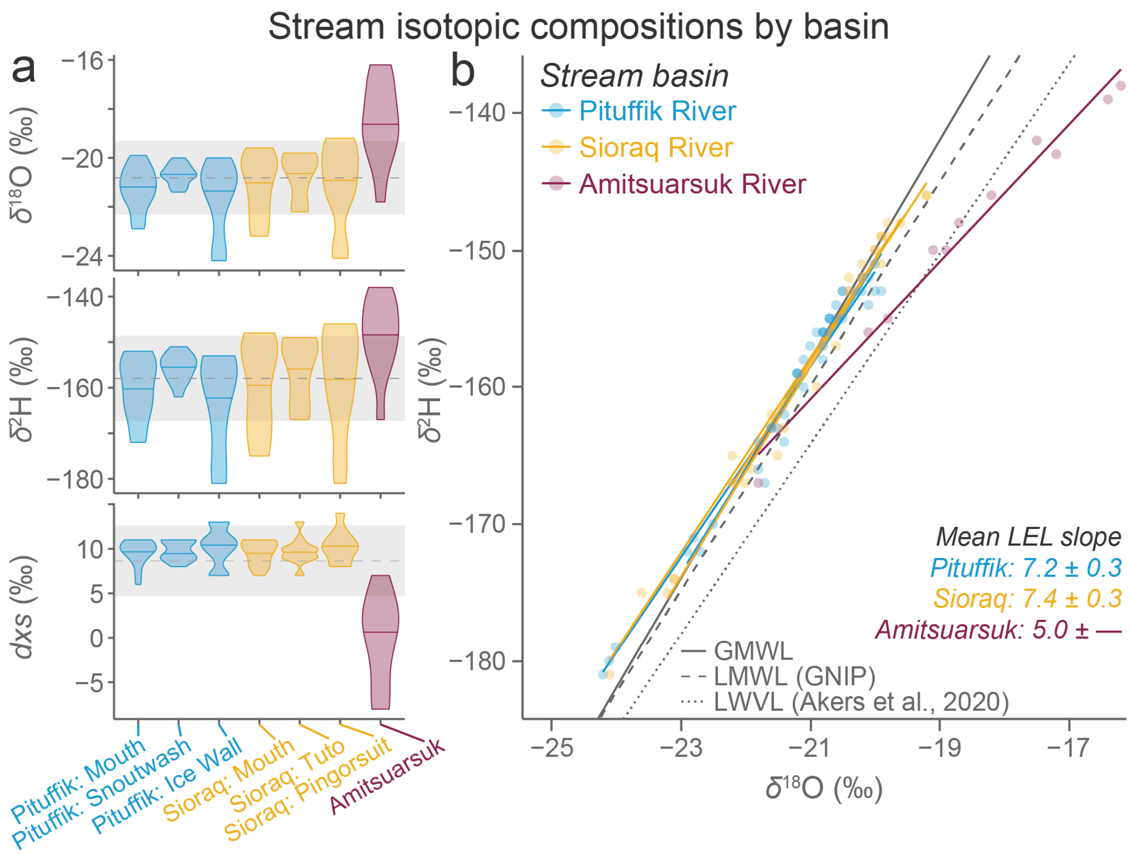

Figure 9. Spatial variability in the isotopic composition of Pituffik streams. Three frequent sampling sites each existed for the Pituffik and Sioraq Rivers while Amitsuarsuk River was sampled less regularly at different points along its entire stretch. Violin plots (a) show the isotopic distributions of stream water samples grouped by stream sample site. Data are plotted so that the maximum width is equivalent between groups, regardless of sample count. The mean isotopic values ± 1 standard deviation of all samples are shown by the dashed line and gray bar crossing all violins. Within each violin, the median value per site is shown by a solid horizontal line. In (b), δ^2H vs. δ^{18}O is plotted to show local evaporation lines (LELs) for each stream sampling site colored by stream basin. LEL slope value means and 95% confidence intervals of the means are displayed for each stream basin. Note that because Amitsuarsuk River was irregularly sampled at points along its main stem, it only has a single LEL and no confidence interval of the mean.

These differences in evaporation's isotopic impact on the streams directly result from the spatial differences in where the streams primarily source their water. The headwaters of all major tributaries of the Pituffik and Sioraq are sourced at the GrIS or large permanent snowfields. Unsurprisingly, the *dxs* values at the Pituffik and Sioraq River sites are never lower than +6 ‰ and fall within values that we observed in snow and ice on the landscape (Figure 3a, Figure 9a). This *dxs* match supports that snow and ice meltwater is consistently the primary water source for the Pituffik and Sioraq Rivers and that evaporation does not substantially impact the water supplying these streams after its original precipitation deposition. For these two streams, the volume and speed of flow from snowpack and GrIS melt apparently overwhelms any other contribution from lakes or other surface waters that would have lower *dxs* values due to evaporative water losses or from summer precipitation.

In contrast, the Amitsuarsuk River has no connection to the GrIS or high elevation snow patches, but it does directly connect and drain several of the main lakes (Figure S4). The isotopically heavier δ^{18}O and δ^{2}H values and markedly lower *dxs* values (–8 to +7 ‰) in the Amitsuarsuk River thus result from the stream sourcing its water primarily from lakes experiencing considerable evaporative water loss (Section 5). Indeed, the slope of the Amitsuarsuk River's LEL (5.0±0.5, Figure 9b) is within the confidence interval of the downstream lakes LEL slope (4.8±0.6, Figure 5b), confirming that the Amitsuarsuk River's water is carrying the evaporative signal created in the lakes along its course. Additionally, the *dxs* values of the Amitsuarsuk River decrease as summer progresses (Figure S9), mimicking the evaporation-driven isotopic evolution observed in the lakes (Figure 8a–b). This is in particular contrast to the *dxs* evolution of the Pituffik and Sioraq Rivers which lack any consistent and clear *dxs* trend over summer (Figure S9). Finally, the four 2019 samples from the Amitsuarsuk River had lower *dxs* values than all 2018 samples but one, and this also mimics the lake observations where waters had lower *dxs* values in 2019 due to the greater evaporative water loss that occurred that summer (Figure 8c–d). The Pituffik and Sioraq Rivers, in contrast, show no distinct differences in *dxs* between the two summers (Figure S9), confirming the limited impact that evaporation plays in determining the streams' isotopic compositions.

6.2 Temporal variability in stream isotopes

Our frequent sampling of the six sites along the Pituffik and Sioraq Rivers allows us to examine the isotopic evolution of these two streams over the summer thaw season. Similar to our monitoring of Lake Potato and Power Lake, the 2018 summer was almost fully captured while only two weeks were observed in 2019 (Figure 10). However, this 2019 sampling coincided with one of the largest known periods of GrIS surface melt mass loss (Cullather et al., 2020; Sasgen et al., 2020) when the Pituffik and Sioraq Rivers had extremely high discharge rates (Figure S3b, d). As discussed previously, we interpret the isotopic variability in these two streams as lower $\delta^{18}O$ and $\delta^{2}H$ values signifying greater tundra snowpack contribution and higher $\delta^{18}O$ and $\delta^{2}H$ values signifying greater GrIS contribution. The much higher variability and lack of obvious patterns in stream *dxs* values makes their interpretation less certain and possibly more responsive to individual precipitation events.

Similar to our lake spatial analysis, the evolution of stream isotopic compositions over time means that spatial comparison across sites is best performed with samples that were taken close together in date. For comparing water isotopes at the mouths of the Pituffik and Sioraq Rivers, we have eleven dates in 2018 and three dates in 2019 where both sites were sampled within 36 hours of each other. Overall, the mean isotopic difference between the two streams on matched days is small, with the Pituffik River having 0.2 ‰ lower $\delta^{18}O$ and 1 ‰ lower $\delta^{2}H$ values than the Sioraq River and no notable *dxs* difference. Both these streams drain similarly large swaths of tundra and directly source meltwater from the GrIS margin, and it is therefore logical that they have similar isotopic values. The mean isotopic value of all sampled dates for these two streams ($\delta^{18}O = -21.1 \pm 0.3$ ‰, $\delta^{2}H = -159 \pm 2$ ‰, $dxs = 10 \pm 1$ ‰) falls between values for GrIS melt and tundra snowpack, reflecting the joint contributions to streamflow from both sources.

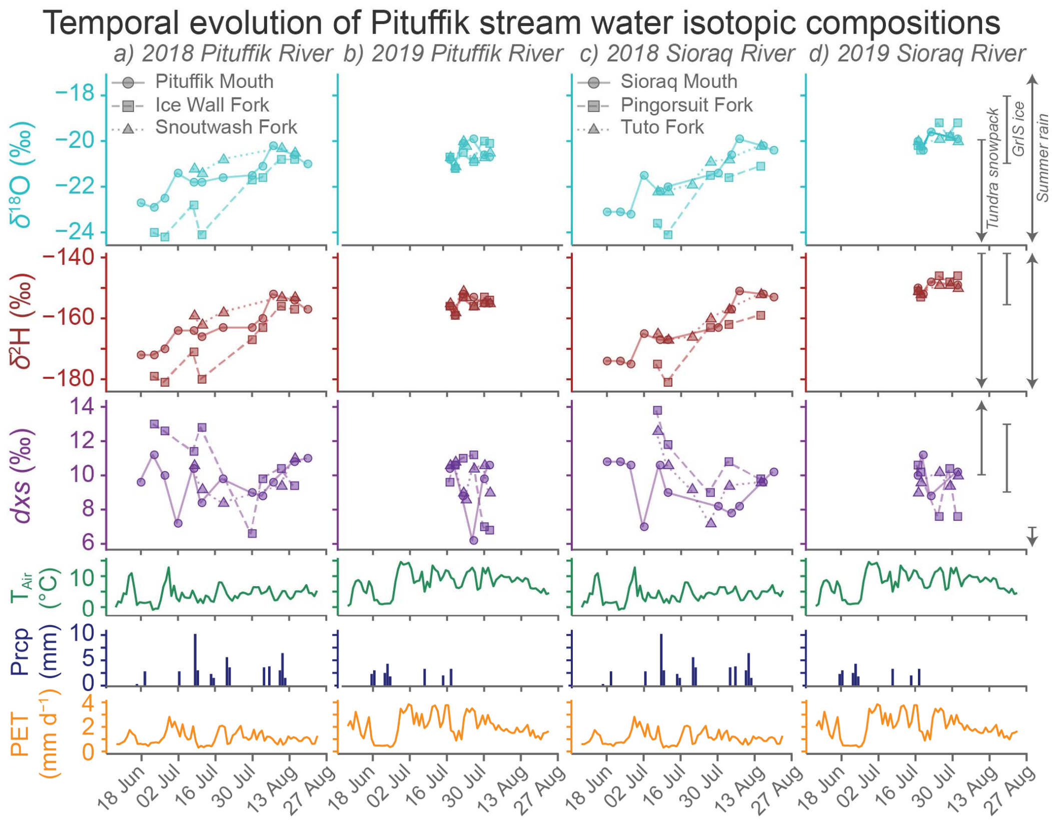

Figure 10. Stream water isotopic value changes along the Pituffik River (a–b) and Sioraq River (c–d) in summers 2018 and 2019. Sampling was performed at three sites on each stream, and different site data are indicated by different icon shapes and line patterns. The daily mean air temperature, precipitation amount, and potential evapotranspiration (Muscari, 2018; Singer et al., 2021; USAF, 2019) for the corresponding summer are provided at bottom for environmental context. The ranges of observed isotopic values in the winter tundra snowpack, the GrIS ice, and summer rain events are shown at far right.

In the early summer, the Ice Wall Fork of the Pituffik River was isotopically lighter than the Pituffik mouth while the Snoutwash Fork was isotopically heavier than the mouth (Figure 10a). Notably, the Ice Wall Fork predominately drains higher elevation plains and moraines than the Snoutwash Fork, and the early season isotopic differences between the forks are likely due to the isotopically light winter tundra snowpack lasting and contributing to streamflow longer in the Ice Wall Fork's watershed. A similar pattern exists for the Sioraq River in early summer (Figure 10c) where the isotopically lighter Pingorsuit Fork drains the highest land elevations on the peninsula (the 800+ m Pingorsuit Massif) while the isotopically heavier Tuto Fork drains a relatively lower elevation region. By late summer, the isotopic composition of each stream's three components converged as very little residual winter tundra snowpack remains and all stream forks sourced the same regionally consistent runoff from glacial melt and precipitation.

Over the 2018 summer, stream water became isotopically heavier at all Pituffik River and Sioraq River sampling sites while *dxs* variability was irregular (Figure 10a, c). A similar general summer increase in $\delta^{18}O$ was also observed on the Sioraq River during summer-long sampling in 2010, 2011, and 2012 (Csank et al., 2019). Unlike the isotopic value increase observed in Lake Potato and Power Lake (Figure 8), the increase in stream isotopic values does not appear to be driven by evaporation because the Pituffik and Sioraq Rivers' *dxs* values do not show a coinciding value decline. Instead, this $\delta^{18}O$ and $\delta^{2}H$ increase represents the shift in stream water contribution from predominantly tundra snowpack meltwater in early summer to predominantly GrIS meltwater in late summer. Over June 2018, the Pituffik and Sioraq watersheds changed from >75% snow-covered to <10% snow-covered with a major snowpack melt event on 14 June when the local air temperature reached 14°C (Copernicus, 2019; USAF, 2019) (Figure S2). Reflecting their tundra snowpack meltwater origin, the streams' isotopic values throughout June were very similar to the values of samples taken directly of snowpack runoff on 14 June, including the first Lake Potato monitoring sample (Figure 8b) taken as this runoff flooded the lake.

The rate of $\delta^{18}O$ and $\delta^{2}H$ increase greatly slowed during July 2018 at the stream mouths (Figure 10a, c) reflecting a stable, relatively low flow system supplied by continued melting of small residual snowpack patches, limited GrIS surface melt, and precipitation events. This stable hydrology was favored by a cool and somewhat wet July 2018 with a mean air temperature of 3.9°C and measurable rain totaling 29 mm that fell on 7 days (Muscari, 2018; USAF, 2019). Some of these rain events were intense for the region, such as the two-day 13.2 mm total that fell on 8–9 July, but an impact from precipitation events is difficult to clearly distinguish in the stream isotopes. Observed summer precipitation $\delta^{18}O$ and $\delta^{2}H$ values are generally isotopically heavier than the early summer stream values and similar to late summer stream values, and therefore some of the overall rise in stream isotopic values over the summer could also be attributed to an increased relative importance of precipitation in the stream flow.

Precipitation may have a more substantial impact on stream *dxs* values. Our sampled summer rain events also had consistently lower *dxs* values than the streams (Figure 3a), and precipitation pulses may help explain some of the stream *dxs* variability, such as the abnormally low *dxs* values observed on 03 July 2018 in both the Pituffik and Sioraq River mouths. High *dxs* values observed in mid-July at the Ice Wall Fork of the Pituffik River and both upper forks of the Sioraq River may have resulted from late melting winter snowpack at these higher elevations or perhaps fresh snow input from a 8–9 July storm. However, most summer precipitation events at Pituffik are very small (< 5 mm), and any direct inflow from precipitation would be heavily mixed with residual snowmelt and thawing active layer water. Also, stream *dxs* variability cannot be entirely due to precipitation pulses because we observe a high degree of *dxs* variability in 2019 when no precipitation was occurring (Figure 10b, d). Overall, we would expect any isotopic impact from precipitation to be short-lived and typically overwhelmed by meltwater from either the tundra snowpack or the GrIS.

Although the sampling period in 2019 was much shorter than 2018, it highlights well a sensitivity of the stream isotopic composition to the season-long weather pattern. Comparing samples taken only between 17 July and 03 August across both years, we observe that the stream sites in 2019 had consistently higher $\delta^{18}O$ and $\delta^{2}H$ values (mean ± 95% confidence interval of each site's differences = +1.1±0.4 ‰ and +9±3 ‰, respectively) but no clear *dxs* difference (+1±1 ‰). We interpret this as the streams having a greater GrIS meltwater component in late July 2019 than late July 2018. Indeed, as previously stated, summer 2019 was much warmer than summer 2018 with a very early loss of the tundra snowpack and limited precipitation (Figure S2). Abnormally high seasonal GrIS surface melt culminated in a near record melt event on 30–31 July 2019 (Cullather et al., 2020) when we observed GrIS meltwater drive extreme Pituffik and Sioraq River discharges that far exceeded 2018 maximum flows and threatened long-established local infrastructure of bridges and roads (Figure S3). The 2019 melt event was also notable for the very low snow cover present on the local GrIS resulting in direct melt of glacial ice across vast expanses. As a result, we consider the stream water during this event to be nearly 100% GrIS sourced and to represent maximum potential meltwater-driven $\delta^{18}O$ and $\delta^{2}H$ values for the Pituffik and Sioraq Rivers.

7 Implications and conclusions

Our comprehensive study of the surface waters of the Pituffik region has important implications for paleoenvironmental studies that use water stable isotopes as proxies for past climate changes. Studies of this nature typically create transfer functions from modern observations of stable isotopes and environmental parameters to convert isotopic values archived in sediment or faunal remains into reconstructed climate histories (Van Hardenbroek et al., 2018). However, observational datasets are usually limited in scope by logistics and cost, particularly in the remote Arctic, and thus datasets collected over short time windows and/or limited spatial coverage are commonly assumed out of necessity to represent norms (e.g., Lasher et al., 2017, 2020; McFarlin et al., 2019). However, our study reveals that surface water isotopic values in the Pituffik region vary greatly in both time and space, particularly for lakes. As a result, a water sample taken on a single date at one body of water can neither be assumed representative for other regional water bodies nor assumed representative of the sampled body of water's isotopic composition at other dates throughout the season or even the same date in a different year.

However, this does not mean that Arctic surface water isotopes are inherently too complex to perform as climate proxies. Based on our study's findings, we offer the following advice on how best to perform the modern water isotope sampling required to produce paleoenvironmental transfer functions in the Arctic. First, it is critical that water samples are taken from the source of the archived isotopes to be studied rather than assuming that samples from other water sources in the region will be similar and applicable. As lakes are the most likely source of an archived sediment record, this means that the specific lake of paleoenvironment study must be the focus of the modern sampling. Differences in lake type and hydrological connectivity can produce wildly different isotopic compositions even between lakes located <500 m apart (Figure 6a), and therefore isotope-climate relationships determined for a lake should only be applied to that specific lake alone.

Secondly, sampling should ideally take place multiple times over a full thaw season in order to capture and model the seasonal evolution and environmental sensitivity of the water isotopes. In particular, lake water samples taken only on a single date risk being substantially different in isotopic composition from other dates and from the summer-long mean. However, few Arctic field campaigns can perform season-long sampling. For time-limited sampling, we recommend taking multiple samples across whatever time is available, particularly before and after major weather events to determine sensitivity to precipitation and surface flow changes. Sampling during early summer must acknowledge that snowpack melt and residual lake ice cover greatly skew lake isotopic compositions relative to their more consistent middle and late summer values.

Related to this point, monitoring should ideally occur at not only the lake where the paleoclimate archive is being collected, but also more broadly across other regional lakes. This will allow researchers to establish the regional response to climate variations and determine how representative the chosen lake of focus is within the larger suite of lakes. To obtain an archived isotopic record that broadly tracks regional climate changes, the chosen lake should ideally follow the general trends of the regional set of lakes and avoid extreme sensitivities or unique isotopic and hydrological responses. However, some of these more sensitive or unique lakes may also prove ideal for a study targeting the particular climate parameter to which a lake is most responsive (e.g., targeting an endorheic or small headwater lake for evaporative water loss). Although hydrological parameters do not consistently control isotopic changes across different lake types, these lake type differences may allow us to capture different aspects of environmental change through comparative lake record study (e.g., Thomas et al., 2020). Critically, having the broader spatial context of the regional lake isotopic composition helps prevent misinterpreting or misattributing a lake's isotopic signal and enhances the insight that can be gleaned from a lake's paleoclimate archives.

Thirdly, many studies assume that archived water isotopic values in Arctic lake sediments reflect the local precipitation and thus can be used to reconstruct past precipitation isotope changes. However, our findings suggest that this assumption cannot be broadly applied and must be verified for each lake. Nearly every Pituffik lake shows signs of isotopic alteration from evaporative loss, and many of the lakes that might be considered ideal for paleoenvironmental study (e.g., limited connectivity, small localized watersheds) are the most strongly impacted by evaporation. The isotopic composition of Pituffik lakes also appears to be substantially buffered against change from summer precipitation events, possibly due to the small volume of water that these events contribute relative to the existing lake volumes and the winter snowpack. As a result, the mean summer isotopic value of a lake probably best reflects a residual isotopic signal from the previous end of summer's lake water with major contributions from the prior winter's snowpack and current summer evaporation. Archived lake water isotopes might therefore be more accurately capturing temperature and moisture source changes of autumn and early winter precipitation (i.e., the predominant source of the snowpack) and/or summer temperature and humidity values that drive evaporation rather than changes in summer precipitation isotopes.

Finally, while the many environmental drivers of lake isotopic variability can make it challenging to parse out which exact paleoclimate changes might have led to a given isotopic change in an individual lake, a more consistent response often emerges when comparing climate proxy variability across a suite of lakes in a region (e.g., Cluett & Thomas, 2020; Engstrom et al., 2000; Gibson & Edwards, 2002; Kopec et al., 2018; Shuman & Serravezza, 2017). Given this consistency, collecting and analyzing sediment cores from multiple lakes in a given region would offer the most effective means of confidently capturing a regional climate signal. Increasing the number of cores to collect and analyze obviously brings logistical challenges, but records from multiple lakes not only reduce the uncertainty of identifying environmental drivers of isotopic change but also eliminates the risk than an observed isotopic excursion was simply a fluke incident that only affected a single lake.

Our Pituffik results offer one example of the potential power of a regional lake suite approach. Pituffik lakes displayed a common isotopic response to more evaporative summer conditions in 2019 relative to 2018 (Figure 8c–d) that were favored by a shift to a strongly negative North Atlantic Oscillation phase in 2019. The consistent isotopic response across the peninsula's lakes strongly supports a connection to a regional to synoptic scale environmental driver like the North Atlantic Oscillation, but arguing the same climate connection based on an isotopic record from only a single lake would be much less certain due to the potential interference of local lake-specific influences. Looking farther afield, similarly consistent responses between lake isotopic compositions and the North Atlantic Oscillation were also reported from a study of multiple lakes in west Greenland (Kopec et al., 2018), suggesting that lake water isotopes along the western coast of Greenland might be used to produce a record of past air pressure variability over the GrIS. In this manner, placing a greater focus on examining lake isotopic records as regional sets rather than individually has much underutilized potential for Arctic paleoenvironmental and hydrological research.

Overall, our study displays the high potential value of hydrological insight gained through intensive field isotopic sampling at a landscape scale. The isotopic compositions in our dataset encompass a nearly full complement of natural surface water types, and they function as a valuable base of comparison for isotopic studies in other Arctic water systems. The number, diversity, and frequency of lakes sampled in our work is, to our best knowledge, unprecedented for the High Arctic latitude of Pituffik and seldom achieved elsewhere in the Arctic and subarctic. Importantly, the numerous stream, surface flow, and snow/ice samples taken alongside the lake samples provide critical environmental context for understanding the expression and evolution of the lake water isotopes. Finally, our large comprehensive dataset can not only aid those investigating past and modern hydrologic systems, but also serve as a foundational isotopic reference point to quantify future environmental changes. We strongly believe that isotopic datasets such as ours from Pituffik will increasingly provide valuable, quantifiable markers of past conditions that can be directly compared with future isotopic samples to track rapid Arctic environmental change in a globally warming Earth.

Acknowledgments

The authors declare no conflicts of interest regarding this research or publication. This project was funded by NSF Arctic Observing Network-ITEX 1504141 and Arctic Observing Network- EAGER MOSAiC 1852614 and supported in part by the inaugural UArctic Research Chairship to Jeff Welker. We greatly thank the assistance of the United States Air Force, the 821st Air Base Group at Pituffik Space Base/Thule Air Base, Vectrus, and Polar Field Services for the logistical and hosting support throughout this research. We thank Giovanni Muscari for graciously providing local Pituffik meteorological data. Special thanks go to the 821st Weather Squadron for meteorological data collection and to Hannah Bailey, Tarja Törmänen, Aino Erkinaro, and Kaisa-Riikka Mustonen for assisting with isotope analysis. We also thank Niels Jákup Korsgaard for his help in finding and accessing archived aerial photographs for Pituffik.

Availability statement

All data and code used in this article’s analyses and figure creation, including the full water isotopic dataset, are openly available online in an Zenodo repository via https://doi.org/10.5281/zenodo.8262359 (Akers et al., 2023a) and also through PANGAEA (*repository submission currently in progress*). Geospatial data created for the Pituffik region and used in this article’s analyses and figures are also openly available either as part of a new geospatial database available on GitHub via https://doi.org/10.5281/zenodo.8256756 (Akers et al., 2023b) or through existing resources also available online (Copernicus, 2019; Howat, 2019; Korsgaard et al., 2016; Porter et al., 2019).

References

Akers, P. D., Kopec, B. G., Mattingly, K. S., Klein, E. S., Causey, D., & Welker, J. M. (2020). Baffin Bay sea ice extent and synoptic moisture transport drive water vapor isotope (δ^{18}O, δ^{2}H, and deuterium excess) variability in coastal northwest Greenland. *Atmospheric Chemistry and Physics*, *20*(22), 13929–13955. https://doi.org/10.5194/acp-20-13929-2020

Akers, P. D., Kopec, B. G., Klein, E. S., & Welker, J. M. (2023a). Pituffik 2018–2019 surface water stable isotope data and analyses (v1.1) (Version v1.1) [Data set]. Zenodo. https://doi.org/10.5281/zenodo.8262359

Akers, P. D., Kopec, B. G., Klein, E. S., & Welker, J. M. (2023b). Pituffik, Greenland, hydrological geopackage (v1.0.1) (Version v1.0.1) [Data set]. Zenodo. https://doi.org/10.5281/zenodo.8256756

Amstrup, N. (1997). Grønland under den kolde krig. Dansk og amerikansk sikkerhedspolitik 1945-1968,1-2, 1-2, København: Dansk Udenrigspolitisk Institut, 1997, 614+473 s., kr. 395,00. *Politica*, *29*(2), 215. https://doi.org/10.7146/politica.v29i2.68132

Anderson, L., Birks, J., Rover, J., & Guldager, N. (2013). Controls on recent Alaskan lake changes identified from water isotopes and remote sensing. *Geophysical Research Letters*, *40*(13), 3413–3418. https://doi.org/10.1002/grl.50672

Anderson, N. J., Saros, J. E., Bullard, J. E., Cahoon, S. M. P., McGowan, S., Bagshaw, E. A., et al. (2017). The Arctic in the Twenty-First Century: changing biogeochemical linkages across a paraglacial landscape of Greenland. *BioScience*, *67*(2), 118–133. https://doi.org/10.1093/biosci/biw158

Arp, C. D., Jones, B. M., Liljedahl, A. K., Hinkel, K. M., & Welker, J. M. (2015). Depth, ice thickness, and ice-out timing cause divergent hydrologic responses among Arctic lakes. *Water Resources Research*, *51*(12), 9379–9401. https://doi.org/10.1002/2015WR017362

Bailey, H., Hubbard, A., Klein, E. S., Mustonen, K.-R., Akers, P. D., Marttila, H., & Welker, J. M. (2021). Arctic sea-ice loss fuels extreme European snowfall. *Nature Geoscience*, *14*(5), 283–288. https://doi.org/10.1038/s41561-021-00719-y

Bhatt, U. S., Walker, D. A., Raynolds, M. K., Bieniek, P. A., Epstein, H. E., Comiso, J. C., et al. (2017). Changing seasonality of panarctic tundra vegetation in relationship to climatic variables. *Environmental Research Letters*, *12*(5), 055003.

Bintanja, R., & Selten, F. M. (2014). Future increases in Arctic precipitation linked to local evaporation and sea-ice retreat. *Nature*, *509*(7501), 479-+. https://doi.org/10.1038/nature13259

Bonne, J.-L., Masson-Delmotte, V., Cattani, O., Delmotte, M., Risi, C., Sodemann, H., & Steen-Larsen, H. C. (2014). The isotopic composition of water vapour and precipitation in Ivittuut, southern Greenland. *Atmospheric Chemistry and Physics*, *14*(9), 4419–4439. https://doi.org/10.5194/acp-14-4419-2014

Bowen, G. J., Putman, A., Brooks, J. R., Bowling, D. R., Oerter, E. J., & Good, S. P. (2018). Inferring the source of evaporated waters using stable H and O isotopes. *Oecologia*, *187*(4), 1025–1039. https://doi.org/10.1007/s00442-018-4192-5

Box, J. E., Colgan, W. T., Christensen, T. R., Schmidt, N. M., Lund, M., Parmentier, F.-J. W., et al. (2019). Key indicators of Arctic climate change: 1971–2017. *Environmental Research Letters*, *14*(4), 045010. https://doi.org/10.1088/1748-9326/aafc1b

Buchwal, A., Sullivan, P. F., Macias-Fauria, M., Post, E., Myers-Smith, I. H., Stroeve, J. C., et al. (2020). Divergence of Arctic shrub growth associated with sea ice decline. *Proceedings of the National Academy of Sciences*, *117*(52), 33334–33344. https://doi.org/10.1073/pnas.2013311117

Burnham, K. K., Sinnett, D. R., Johnson, J. A., Burnham, J. L., Baroch, J. A., & Konkel, B. W. (2014). New species records and changes in abundance of waterfowl in northwest Greenland. *Polar Biology*, *37*(9), 1289–1300. https://doi.org/10.1007/s00300-014-1520-z

Casado, M., Landais, A., Masson-Delmotte, V., Genthon, C., Kerstel, E., Kassi, S., et al. (2016). Continuous measurements of isotopic composition of water vapour on the EastAntarctic Plateau. *Atmospheric Chemistry and Physics*, *16*(13), 8521–8538. https://doi.org/10.5194/acp-16-8521-2016

Clark, E. F. (1965). *Camp Century: Evolution of concept and history of design, construction, and performance* (Technical Report No. 174). Hanover, New Hampshire, USA: U.S. Army Material Command, Cold Regions Research and Engineering Laboratory.

Clark, I. D., & Fritz, P. (1997). *Environmental Isotopes in Hydrogeology* (1st ed.). Boca Raton: CRC Press. Retrieved from https://doi.org/10.1201/9781482242911

Cluett, A. A., & Thomas, E. K. (2020). Resolving combined influences of inflow and evaporation on western Greenland lake water isotopes to inform paleoclimate inferences. *Journal of Paleolimnology*, *63*(4), 251–268. https://doi.org/10.1007/s10933-020-00114-4

Colgan, W., Machguth, H., MacFerrin, M., Colgan, J. D., van As, D., & MacGregor, J. A. (2016). The abandoned ice sheet base at Camp Century, Greenland, in a warming climate. *Geophysical Research Letters*, *43*(15), 8091–8096. https://doi.org/10.1002/2016GL069688

Copernicus. (2019). Sentinel-2 data, Sentinel Hub. Retrieved August 15, 2019, from https://www.sentinel-hub.com/

Corbett, L. B., Bierman, P. R., Lasher, G. E., & Rood, D. H. (2015). Landscape chronology and glacial history in Thule, northwest Greenland. *Quaternary Science Reviews*, *109*, 57–67. https://doi.org/10.1016/j.quascirev.2014.11.019

Craig, H. (1961). Isotopic variations in meteoric waters. *Science*, *133*(3465), 1702.

Craig, H., & Gordon, L. I. (1965). Deuterium and oxygen 18 variations in the ocean and the marine atmosphere. In E. Tongiorgi (Ed.), *Stable Isotopes in Oceanographic Studies and Paleotemperatures* (pp. 9–130). Spoleto, Italy: Consiglio nazionale delle ricerche, Laboratiorio di geologica nucleare.

Csank, A. Z., Czimczik, C. I., Xu, X., & Welker, J. M. (2019). Seasonal patterns of riverine carbon sources and export in NW Greenland. *Journal of Geophysical Research: Biogeosciences*, *124*(4), 840–856. https://doi.org/10.1029/2018JG004895

Cullather, R. I., Andrews, L. C., Croteau, M. J., Digirolamo, N. E., Hall, D. K., Lim, Y., et al. (2020). Anomalous circulation in July 2019 resulting in mass loss on the Greenland ice sheet. *Geophysical Research Letters*, *47*(17), e2020GL08726. https://doi.org/10.1029/2020GL087263

Cuyler, C., Virk, K. S., Clausen, T. B., Jensen, F. H., Born, E. W., Laidre, K. L., & Wiig, Ø. (2022). *2017 status muskoxen (Ovibos moschatus) Cape Atholl, Thule region Greenland* (Technical Report No. 104) (p. 60). Pinngortitaleriffik – Greenland Institute of Natural Resources. Retrieved from 87-91214-81-5

Daniels, W. C., Russell, J. M., Morrill, C., Longo, W. M., Giblin, A. E., Holland-Stergar, P., et al. (2021). Lacustrine leaf wax hydrogen isotopes indicate strong regional climate feedbacks in Beringia since the last ice age. *Quaternary Science Reviews*, *269*, 107130. https://doi.org/10.1016/j.quascirev.2021.107130

Dansgaard, W. (1964). Stable isotopes in precipitation. *Tellus*, *16*(4), 436–468. https://doi.org/10.1111/j.2153-3490.1964.tb00181.x

Dansgaard, W., Johnsen, S. J., Møller, J., & Langway, C. C. (1969). One thousand centuries of climatic record from Camp Century on the Greenland Ice Sheet. *Science*, *166*(3903), 377.

Davies, W. E., & Reitzel, C. A. (1963). *Geology of the North Star Bugt Area, Northwest Greenland*. C.A. Reitzels Forlag. Retrieved from https://books.google.ie/books?id=OCA7xgEACAAJ

Davis, R. M. (1966). *Design, construction and performance data of utility systems, Thule Air Base* (Special Report No. 95) (pp. 1–62). Hanover, New Hampshire, USA: U.S. Army Material Command, Cold Regions Research and Engineering Laboratory.

Engstrom, D. R., Fritz, S. C., Almendinger, J. E., & Juggins, S. (2000). Chemical and biological trends during lake evolution in recently deglaciated terrain. *Nature*, *408*(6809), 161–166. https://doi.org/10.1038/35041500

Eriksson, M., Holm, E., Roos, P., & Dahlgaard, H. (2004). Distribution and flux of Pu-238, Pu-239, Pu-240, Am-241, Cs-137 and Pb-210 to high arctic lakes in the Thule district (Greenland). *Journal of Environmental Radioactivity*, *75*(3), 285–299. https://doi.org/10.1016/j.jenvrad.2003.12.007

Farquharson, L. M., Romanovsky, V. E., Cable, W. L., Walker, D. A., Kokelj, S. V., & Nicolsky, D. (2019). Climate change drives widespread and rapid thermokarst development in very cold permafrost in the Canadian High Arctic. *Geophysical Research Letters*, *46*(12), 6681–6689. https://doi.org/10.1029/2019GL082187

Funder, S. (1990). Late Quaternary stratigraphy and glaciology in the Thule area, Northwest Greenland (p. 64). Museum Tusculanum Press.

Gat, J. R. (1996). Oxygen and hydrogen isotopes in the hydrologic cycle. *Annual Review of Earth and Planetary Sciences*, *24*(1), 225–262.

Gibson, J. J. (2002). Short-term evaporation and water budget comparisons in shallow Arctic lakes using non-steady isotope mass balance. *Journal of Hydrology*, *264*(1), 242–261. https://doi.org/10.1016/S0022-1694(02)00091-4

Gibson, J. J., & Edwards, T. W. D. (2002). Regional water balance trends and evaporation-transpiration partitioning from a stable isotope survey of lakes in northern Canada. *Global Biogeochemical Cycles*, *16*(2). https://doi.org/10.1029/2001GB001839

Gibson, J. J., & Reid, R. (2014). Water balance along a chain of tundra lakes: A 20-year isotopic perspective. *Journal of Hydrology*, *519*, 2148–2164. https://doi.org/10.1016/j.jhydrol.2014.10.011

Gibson, J. J., Reid, R., & Spence, C. (1998). A six-year isotopic record of lake evaporation at a mine site in the Canadian subarctic: results and validation. *Hydrological Processes*, *12*(10–11), 1779–1792. https://doi.org/10.1002/(SICI)1099-1085(199808/09)12:10/11<1779::AID-HYP694>3.0.CO;2-7

Gibson, J. J., Edwards, T. W. D., & Prowse, T. D. (1999). Pan-derived isotopic composition of atmospheric water vapour and its variability in northern Canada. *Journal of Hydrology*, *217*(1–2), 55–74. https://doi.org/10.1016/S0022-1694(99)00015-3

Gibson, J. J., Birks, S. J., & Yi, Y. (2016). Stable isotope mass balance of lakes: a contemporary perspective. *Quaternary Science Reviews*, *131*, 316–328. https://doi.org/10.1016/j.quascirev.2015.04.013

Gimeno, L., Vázquez, M., Eiras-Barca, J., Sorí, R., Algarra, I., & Nieto, R. (2019). Atmospheric moisture transport and the decline in Arctic Sea ice. *WIREs Climate Change*, *10*(4). https://doi.org/10.1002/wcc.588

Gonfiantini, R. (1986). Environmental isotopes in lake studies. In P. Fritz & J. C. Fontes (Eds.), *Handbook of environmental isotope geochemistry: the terrestrial environment* (pp. 113–168). New York: Elsevier.

Gronnow, B. (2016). Living at a High Arctic polynya: Inughuit settlement and subsistence around the North Water during the Thule Station Period, 1910-53. *Arctic*, *69*(1). https://doi.org/10.14430/arctic4573

Hansen, B. L., & Langway, C. C. (1966). Deep core drilling in ice and core analysis at Camp Century, Greenland, 1961–66. *Antarctic Journal of the United States*, *1*(5), 207–208.

Hastrup, K., Andersen, A. O., Grønnow, B., & Heide-Jørgensen, M. P. (2018). Life around the North Water ecosystem: Natural and social drivers of change over a millennium. *Ambio*, *47*(2), 213–225. https://doi.org/10.1007/s13280-018-1028-9

Hauser, D. D. W., Whiting, A. V., Mahoney, A. R., Goodwin, J., Harris, C., Schaeffer, R. J., et al. (2021). Co-production of knowledge reveals loss of Indigenous hunting opportunities in the face of accelerating Arctic climate change. *Environmental Research Letters*, *16*(9), 095003. https://doi.org/10.1088/1748-9326/ac1a36

Heide-Jørgensen, M. P., Sinding, M. H. S., Nielsen, N. H., Rosing-Asvid, A., & Hansen, R. G. (2016). Large numbers of marine mammals winter in the North Water polynya. *Polar Biology*, *39*(9), 1605–1614.

Hiltunen, T. A., Stien, A., Väisänen, M., Ropstad, E., Aspi, J. O., & Welker, J. M. (2022). Svalbard reindeer winter diets: Long-term dietary shifts to graminoids in response to a changing climate. *Global Change Biology*, *28*(23), 7009–7022. https://doi.org/10.1111/gcb.16420

Historiske Kort. (2023). Historiske Kort: Flyfotos [Data set]. Styrelsen for Dataforsyning og Infrastruktur. Retrieved from https://historiskekort.dk/

Howat, I. M. (2019). MEaSUREs Greenland Ice Mapping Project (GIMP) Land Ice and Ocean Classification Mask, Version 1, 90 m x 90 m. *NASA NSIDC Distributed Active Archive Center*. https://doi.org/10.5067/B8X58MQBFUPA

Howat, I. M., Negrete, A., & Smith, B. E. (2014). The Greenland Ice Mapping Project (GIMP) land classification and surface elevation data sets. *The Cryosphere*, *8*(4), 1509–1518.

IAEA/WMO. (2022). Global Network of Isotopes in Precipitation. The GNIP Database. Accessible at: https://nucleus.iaea.org/wiser.

Jenness, D. (1925). A new Eskimo culture in Hudson Bay. *Geographical Review*, *15*(3), 428–437. https://doi.org/10.2307/208564

Jespersen, R. G., Leffler, A. J., Oberbauer, S. F., & Welker, J. M. (2018). Arctic plant ecophysiology and water source utilization in response to altered snow: isotopic (δ18O and δ2H) evidence for meltwater subsidies to deciduous shrubs. *Oecologia*, *187*(4), 1009–1023. https://doi.org/10.1007/s00442-018-4196-1

Jespersen, R. G., Leffler, A. J., Väisänen, M., & Welker, J. M. (2022). Resistance and change in a High Arctic ecosystem, NW Greenland: Differential sensitivity of ecosystem metrics to 15 years of experimental warming and wetting. *Global Change Biology*, *28*(5), 1853–1869. https://doi.org/10.1111/gcb.16027

Jonsson, C. E., Leng, M. J., Rosqvist, G. C., Seibert, J., & Arrowsmith, C. (2009). Stable oxygen and hydrogen isotopes in sub-Arctic lake waters from northern Sweden. *Journal of Hydrology*, *376*(1–2), 143–151. https://doi.org/10.1016/j.jhydrol.2009.07.021

Kendall, C., & McDonnell, J. J. (1998). *Isotope Tracers in Catchment Hydrology* (1st ed.). Amsterdam, Netherlands: Elsevier. Retrieved from https://doi.org/10.1016/C2009-0-10239-8

Kjellman, S. E., Thomas, E. K., & Schomacker, A. (2022). Arctic and sub-Arctic lake water δ^2H and δ^{18}O along a coastal-inland transect: Implications for interpreting water isotope proxy records. *Journal of Hydrology*, *607*, 127556. https://doi.org/10.1016/j.jhydrol.2022.127556

Kopec, B. G., Feng, X., Posmentier, E. S., Chipman, J. W., & Virginia, R. A. (2018). Use of principal component analysis to extract environmental information from lake water isotopic compositions. *Limnology and Oceanography*, *63*(3), 1340–1354. https://doi.org/10.1002/lno.10776

Kopec, B. G., Lauder, A. M., Posmentier, E. S., & Feng, X. (2019). The diel cycle of water vapor in west Greenland. *Journal of Geophysical Research: Atmospheres*, *119*(15), 9386–9399.

Korsgaard, N. J., Nuth, C., Khan, S. A., Kjeldsen, K. K., Bjørk, A. A., Schomacker, A., & Kjær, K. H. (2016). Digital elevation model and orthophotographs of Greenland based on aerial photographs from 1978–1987. *Scientific Data*, *3*(1), 160032. https://doi.org/10.1038/sdata.2016.32

Lasher, G. E., Axford, Y., McFarlin, J. M., Kelly, M. A., Osterberg, E. C., & Berkelhammer, M. B. (2017). Holocene temperatures and isotopes of precipitation in northwest Greenland recorded in lacustrine organic materials. *Quaternary Science Reviews*, *170*, 45–55. https://doi.org/10.1016/j.quascirev.2017.06.016

Lasher, G. E., Axford, Y., Masterson, A. L., Berman, K., & Larocca, L. J. (2020). Holocene temperature and landscape history of southwest Greenland inferred from isotope and geochemical lake sediment proxies. *Quaternary Science Reviews*, *239*, 106358. https://doi.org/10.1016/j.quascirev.2020.106358

Leffler, A. J., & Welker, J. M. (2013). Long-term increases in snow pack elevate leaf N and photosynthesis in Salix arctica: Responses to a snow fence experiment in the High Arctic of NW Greenland. *Environmental Research Letters*, *8*(2), 025023.

Leng, M. J., & Anderson, N. J. (2003). Isotopic variation in modern lake waters from western Greenland. *The Holocene*, *13*(4), 605–611. https://doi.org/10.1191/0959683603hl620rr

Linderholm, H. W., Nicolle, M., Francus, P., Gajewski, K., Helama, S., Korhola, A., et al. (2018). Arctic hydroclimate variability during the last 2000 years: Current understanding and research challenges. *Climate of the Past*, *14*(4), 473–514. https://doi.org/10.5194/cp-14-473-2018

Lupascu, M., Welker, J. M., Seibt, U., Maseyk, K., Xu, X., & Czimczik, C. I. (2014). High Arctic wetting reduces permafrost carbon feedbacks to climate warming. *Nature Climate Change*, *4*(1), 51–55. https://doi.org/10.1038/NCLIMATE2058

MacDonald, L. A., Wolfe, B. B., Turner, K. W., Anderson, L., Arp, C. D., Birks, S. J., et al. (2017). A synthesis of thermokarst lake water balance in high-latitude regions of North America from isotope tracers. *Arctic Science*, *3*(2), 118–149. https://doi.org/10.1139/as-2016-0019

MacGregor, J. A., Fahnestock, M. A., Colgan, W. T., Larsen, N. K., Kjeldsen, K. K., & Welker, J. M. (2020). The age of surface-exposed ice along the northern margin of the Greenland Ice Sheet. *Journal of Glaciology*, *66*(258), 667–684. https://doi.org/10.1017/jog.2020.62

McFarlin, J. M., Axford, Y., Masterson, A. L., & Osburn, M. R. (2019). Calibration of modern sedimentary δ2H plant wax-water relationships in Greenland lakes. *Quaternary Science Reviews*, *225*, 105978. https://doi.org/10.1016/j.quascirev.2019.105978

Mellat, M., Bailey, H., Mustonen, K.-R., Marttila, H., Klein, E. S., Gribanov, K., et al. (2021). Hydroclimatic controls on the isotopic (δ^{18}O, δ^{2}H, d-excess) traits of pan-Arctic summer rainfall events. *Frontiers in Earth Science*, *9*, 651731. https://doi.org/10.3389/feart.2021.651731

Merlivat, L., & Jouzel, J. (1979). Global climatic interpretation of the deuterium-oxygen 18 relationship for precipitation. *Journal of Geophysical Research: Oceans*, *84*(C8), 5029–5033. https://doi.org/10.1029/JC084iC08p05029

Mosbech, A., Johansen, K. L., Davidson, T. A., Appelt, M., Grønnow, B., Cuyler, C., et al. (2018). On the crucial importance of a small bird: The ecosystem services of the little auk (Alle alle) population in Northwest Greenland in a long-term perspective. *Ambio*, *47*(2), 226–243. https://doi.org/10.1007/s13280-018-1035-x

Mote, T. L. (2020, February 26). MEaSUREs Greenland Surface Melt Daily 25 km EASE-Grid 2.0, version 1. NASA National Snow and Ice Data Center. Retrieved from https://doi.org/10.5067/MEASURES/CRYOSPHERE/nsidc-0533.001

Muhic, F., Ala-Aho, P., Noor, K., Welker, J. M., Klöve, B., & Marttila, H. (2023). Flushing or mixing? Stable water isotopes reveal differences in Arctic forest and peatland soil water seasonality. *Hydrological Processes*, *37*(1), e14811. https://doi.org/10.1002/hyp.14811

Müller, L., Horwath, M., Scheinert, M., Mayer, C., Ebermann, B., Floricioiu, D., et al. (2021). Surges of Harald Moltke Bræ, north-western Greenland: seasonal modulation and initiation at the terminus. *The Cryosphere*, *15*(7), 3355–3375. https://doi.org/10.5194/tc-15-3355-2021

Muscari, G. (2018). Ground meteorological data (T, P, RH) obtained during the YOPP SOP in early 2018 at Thule Air Base, Greenland. *Istituto Nazionale Di Geofisica e Vulcanologia, Roma, Italy, PANGAEA, Https://Doi.Org/10.1594/PANGAEA.895059*.

Nghiem, S. V., Hall, D. K., Mote, T. L., Tedesco, M., Albert, M. R., Keegan, K., et al. (2012). The extreme melt across the Greenland ice sheet in 2012. *Geophysical Research Letters*, *39*(20). https://doi.org/10.1029/2012gl053611

Nichols, R. L. (1953). Geomorphic observations at Thule, Greenland, and Resolute Bay, Cornwallis Island, NWT. *American Journal of Science*, *251*(4). https://doi.org/10.2475/ajs.251.4.268

Noor, K., Marttila, H., Klöve, B., Welker, J. M., & Ala-aho, P. (2023). The spatiotemporal variability of snowpack and snowmelt water ^{18}O and ^{2}H isotopes in a subarctic catchment. *Water Resources Research*, *59*(1), e2022WR033101. https://doi.org/10.1029/2022WR033101

Oqaasileriffik. (2022). Oqaasileriffik: The Language Secretariat of Greenland. Retrieved May 1, 2022, from https://oqaasileriffik.gl/

Petersen, N. (2008). The Iceman that never came. *Scandinavian Journal of History*, *33*(1), 75–98. https://doi.org/10.1080/03468750701449554

PGC. (2019, August 15). ArcticDEM-Polar Geospatial Center. Retrieved August 15, 2019, from https://www.pgc.umn.edu/data/arcticdem/

Porter, C., Morin, P., Howat, I., Noh, M. J., Bates, B., Peterman, K., et al. (2019). ArcticDEM, *V3.0, Release 7*. https://doi.org/10.7910/DVN/OHHUKH

Putman, A. L., Fiorella, R. P., Bowen, G. J., & Cai, Z. (2019). A global perspective on local meteoric water lines: Meta-analytic insight into fundamental controls and practical constraints. *Water Resources Research*, *55*(8), 6896–6910. https://doi.org/10.1029/2019WR025181

Reeh, N., Thomsen, H. H., Frich, P., & Clausen, H. B. (1990). Stable isotope studies on ice margins in the Thule area. In S. Funder (Ed.), *Late Quaternary stratigraphy and glaciology in the Thule area, Northwest Greenland* (Vol. 22, pp. 47–56). Meddelelser Om Grønland, Geosicence.

Ries, C. J. (2012). On frozen ground: William E. Davies and the military geology of northern Greenland 1952–1960. *The Polar Journal*, *2*(2), 334–357. https://doi.org/10.1080/2154896X.2012.735044

Rozanski, K., Araguás-Araguás, L., & Gonfiantini, R. (1993). Isotopic patterns in modern global precipitation. In *Climate Change in Continental Isotopic Records* (pp. 1–36). Retrieved from https://doi.org/10.1029/GM078p0001

Sasgen, I., Wouters, B., Gardner, A. S., King, M. D., Tedesco, M., Landerer, F. W., et al. (2020). Return to rapid ice loss in Greenland and record loss in 2019 detected by the GRACE-FO satellites. *Communications Earth & Environment*, *1*(1), 8. https://doi.org/10.1038/s43247-020-0010-1

Sauer, P. E., Miller, G. H., & Overpeck, J. T. (2001). Oxygen isotope ratios of organic matter in arctic lakes as a paleoclimate proxy: field and laboratory investigations. *Journal of Paleolimnology*, *25*(1), 43–64. https://doi.org/10.1023/A:1008133523139

Schytt, V. (1955). *Glaciological investigations in the Thule Ramp area* (Sipre Report No. 28) (p. 88). Wilmette, Illinois, USA: Snow, Ice and Permafrost Research Establishment, Corps of Engineers, U.S. Army.

Serreze, M. C., & Barry, R. G. (2011). Processes and impacts of Arctic amplification: A research synthesis. *Global and Planetary Change*, *77*(1–2), 85–96. https://doi.org/10.1016/j.gloplacha.2011.03.004

Shuman, B. N., & Serravezza, M. (2017). Patterns of hydroclimatic change in the Rocky Mountains and surrounding regions since the last glacial maximum. *Quaternary Science Reviews*, *173*, 58–77. https://doi.org/10.1016/j.quascirev.2017.08.012

Singer, M. B., Asfaw, D. T., Rosolem, R., Cuthbert, M. O., Miralles, D. G., MacLeod, D., et al. (2021). Hourly potential evapotranspiration at 0.1° resolution for the global land surface from 1981-present. *Scientific Data*, *8*(1), 224. https://doi.org/10.1038/s41597-021-01003-9

Stansell, N. D., Klein, E. S., Finkenbinder, M. S., Fortney, C. S., Dodd, J. P., Terasmaa, J., & Nelson, D. B. (2017). A stable isotope record of Holocene precipitation dynamics in the Baltic region from Lake Nuudsaku, Estonia. *Quaternary Science Reviews*, *175*, 73–84. https://doi.org/10.1016/j.quascirev.2017.09.013

Swinzow, G. K. (1962). Investigation of Shear Zones in the Ice Sheet Margin, Thule Area, Greenland. *Journal of Glaciology*, *4*(32), 215–229. https://doi.org/10.3189/S0022143000027416

Takahashi, M. (2019). Greenland's Quest for Autonomy and the Political Dynamics Surrounding the Thule Air Base. In M. Takahashi (Ed.), *Influence of Sub-State Actors on National Security: Using Military Bases to Forge Autonomy* (pp. 25–49). https://doi.org/10.1007/978-3-030-01677-7_3

Tedesco, M., & Fettweis, X. (2020). Unprecedented atmospheric conditions (1948–2019) drive the 2019 exceptional melting season over the Greenland ice sheet. *The Cryosphere*, *14*(4), 1209–1223. https://doi.org/10.5194/tc-14-1209-2020

Thomas, E. K., Hollister, K. V., Cluett, A. A., & Corcoran, M. C. (2020). Reconstructing Arctic precipitation seasonality using aquatic leaf wax δ^2H in lakes with contrasting residence times. *Paleoceanography and Paleoclimatology*, *35*(7), e2020PA003886. https://doi.org/10.1029/2020PA003886

USAF. (2019). THU weather observations, Thule Air Base, Greenland. *821 SPTS/OSW, USAF*.

Van Hardenbroek, M., Chakraborty, A., Davies, K. L., Harding, P., Heiri, O., Henderson, A. C. G., et al. (2018). The stable isotope composition of organic and inorganic fossils in lake sediment records: Current understanding, challenges, and future directions. *Quaternary Science Reviews*, *196*, 154–176. https://doi.org/10.1016/j.quascirev.2018.08.003

Verbruggen, F., Heiri, O., Reichart, G. J., Blaga, C., & Lotter, A. F. (2011). Stable oxygen isotopes in chironomid and cladoceran remains as indicators for lake-water δ^{18}O. *Limnology and Oceanography*, *56*(6), 2071–2079. https://doi.org/10.4319/lo.2011.56.6.2071

Vonk, J. E., Tank, S. E., Bowden, W. B., Laurion, I., Vincent, W. F., Alekseychik, P., et al. (2015). Reviews and syntheses: Effects of permafrost thaw on Arctic aquatic ecosystems. *Biogeosciences*, *12*(23), 7129–7167. https://doi.org/10.5194/bg-12-7129-2015

Weiss, E. D. (2001). Cold War under the ice. *Journal of Cold War Studies*, *3*(3), 31–58.

Welhan, J. A., & Fritz, P. (1977). Evaporation pan isotopic behavior as an index of isotopic evaporation conditions. *Geochimica et Cosmochimica Acta*, *41*(5), 682–686. https://doi.org/10.1016/0016-7037(77)90306-4

Wesche, S. D., & Chan, H. M. (2010). Adapting to the impacts of climate change on food security among Inuit in the western Canadian Arctic. *EcoHealth*, *7*(3), 361–373. https://doi.org/10.1007/s10393-010-0344-8

Wilcox, E. J., Wolfe, B. B., & Marsh, P. (2022). Assessing the influence of lake and watershed attributes on snowmelt bypass at thermokarst lakes. *Hydrology and Earth System Sciences*, *26*(23), 6185–6205. https://doi.org/10.5194/hess-26-6185-2022

Wilcox, E. J., Wolfe, B. B., & Marsh, P. (2023). Hydrological, meteorological, and watershed controls on the water balance of thermokarst lakes between Inuvik and Tuktoyaktuk, Northwest Territories, Canada. *Hydrology and Earth System Sciences*, *27*(11), 2173–2188. https://doi.org/10.5194/hess-27-2173-2023

Water Resources Research

Supporting Information for

Evaporation and water sourcing dominate lake and stream isotopic variability across time and space in a High Arctic periglacial landscape

Pete D. Akers[1], Ben G. Kopec[2], Eric S. Klein[3], Jeffrey M. Welker[2,4,5]

[1]Discipline of Geography, School of Natural Sciences, Trinity College Dublin, Dublin, Ireland.

[2]Ecology and Genetics Research Unit, University of Oulu, 90014 Oulu, Finland.

[3]Department of Geological Sciences, University of Alaska Anchorage, Anchorage, AK, USA.

[4]Department of Biological Sciences, University of Alaska Anchorage, Anchorage, AK, USA.

[5]University of the Arctic (UArctic), c/o University of Lapland, 96101 Rovaniemi, Finland.

Contents of this file

Additional Supporting Information (Files uploaded separately)

Figure S1

Introduction

This supporting information contains figures and tables that provide additional visual and numerical context to the main text. Data and code used to produce these figures and tables are listed under the Availability Statement. All photographs in figures were taken by Pete D. Akers.

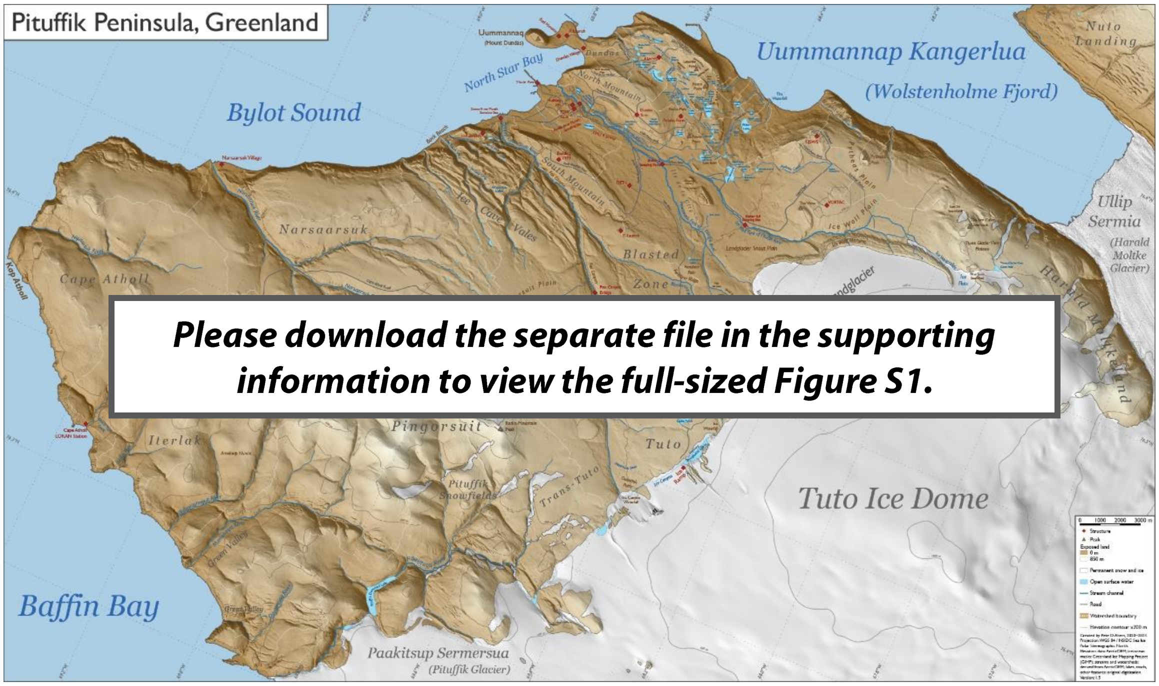

Figure S1 (Separate file). Poster-sized map of the hydrology and land features of the Pituffik Peninsula. Data used to create the map were taken from the Pituffik geospatial database (Akers et al., 2023b) and the cited data within that database. The map was created in QGIS and aesthetic modifications were made using Adobe Illustrator.

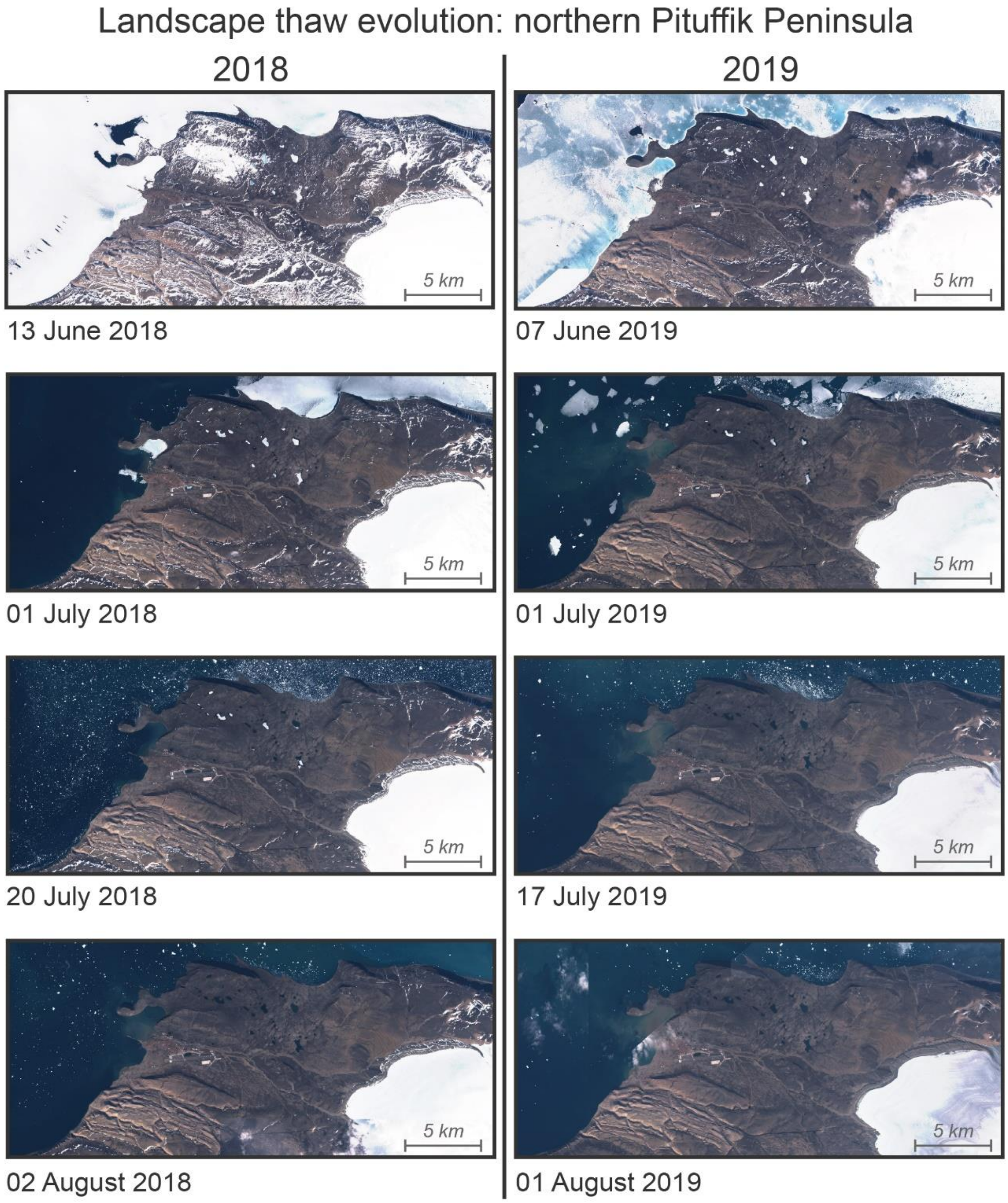

Figure S2. The general thawing progression of the northern Pituffik Peninsula landscape in summers 2018 and 2019. Pituffik Space Base is located at slightly left of direct center, and the Tuto ice dome of the GrIS is present at bottom right. Photographs on the same row are matched by date across the two years, although frequent cloud cover and fog limited same day comparisons in most cases. Note that snow on the landscape and lake ice lasted later into the summer in 2018 than 2019. Additionally, dark GrIS ice is visible in the 01 August 2019 image after an extreme surface melt event of the GrIS removed its snow cover and exposed the underlaying, less reflective ice.

Figure S3. Observed variability in stream flow rates in Pituffik streams in 2018 and 2019. In a), a moderate flow of the Pituffik River occurs in early summer due to melting of the tundra snowpack. In b) the Pituffik River discharges at near maximum rates due to an extreme GrIS surface melt event. For the Sioraq River, flow rates were moderate in early July 2018 under cool conditions and limited GrIS melt (c), but the same site is seen with very high flow on 01 August 2019 (d) during the same extreme GrIS surface melt event as (b). The Amitsuarsuk River has its highest flow rates in early summer when the tundra snowpack melts (not pictured) with lower flows sustained over the rest of summer (e) through precipitation, active layer water thaw, and residual snow patch melt. In contrast to the Pituffik and Sioraq Rivers (b, d), the Amitsuarsuk River's flow was very low during the 2019 extreme GrIS surface melt event (f) as the stream has no connection to the GrIS, and the lack of precipitation and strong evaporation during the 2019 summer suppressed its water supply.

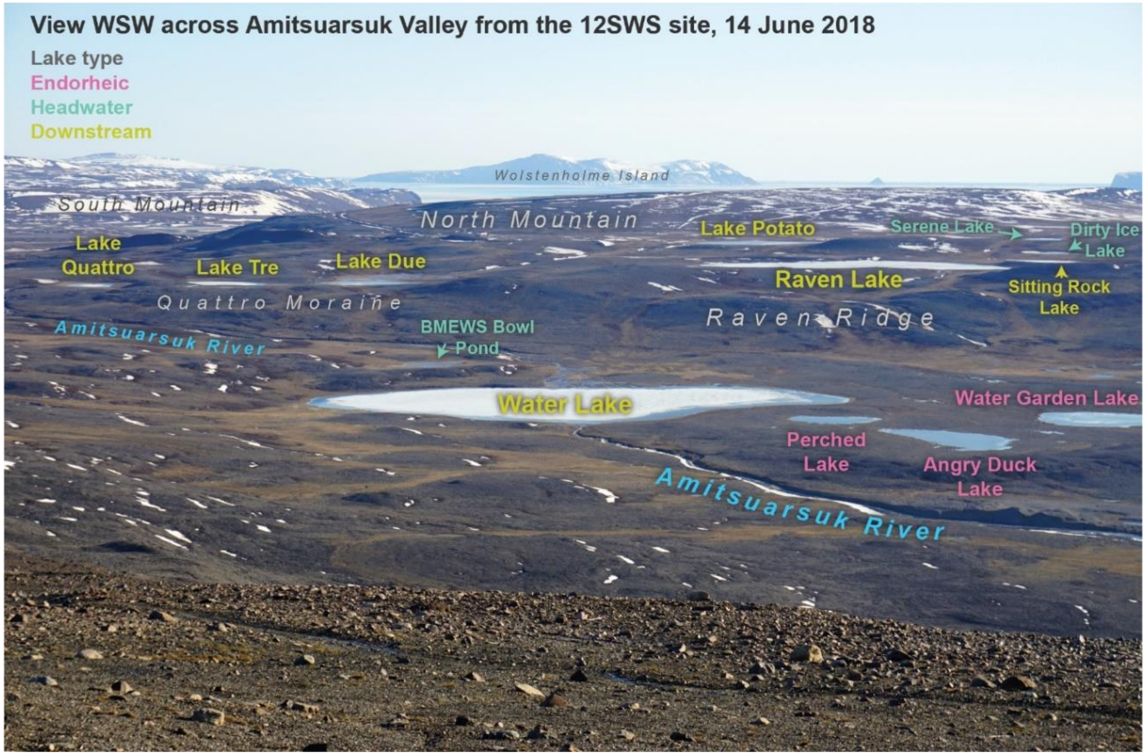

Figure S1. View of the Pituffik landscape and hydrological system around the Amitsuarsuk Valley. Visible lakes are labeled and colored according to their lake type. On the date of the photograph (14 Jun 2018), the tundra snowpack had only recently experienced substantial melt, and most lakes had only started to lose their ice cover. Note, however, that the shallower endorheic and headwater lakes are largely ice-free, likely due to earlier melt of their bedfast ice.

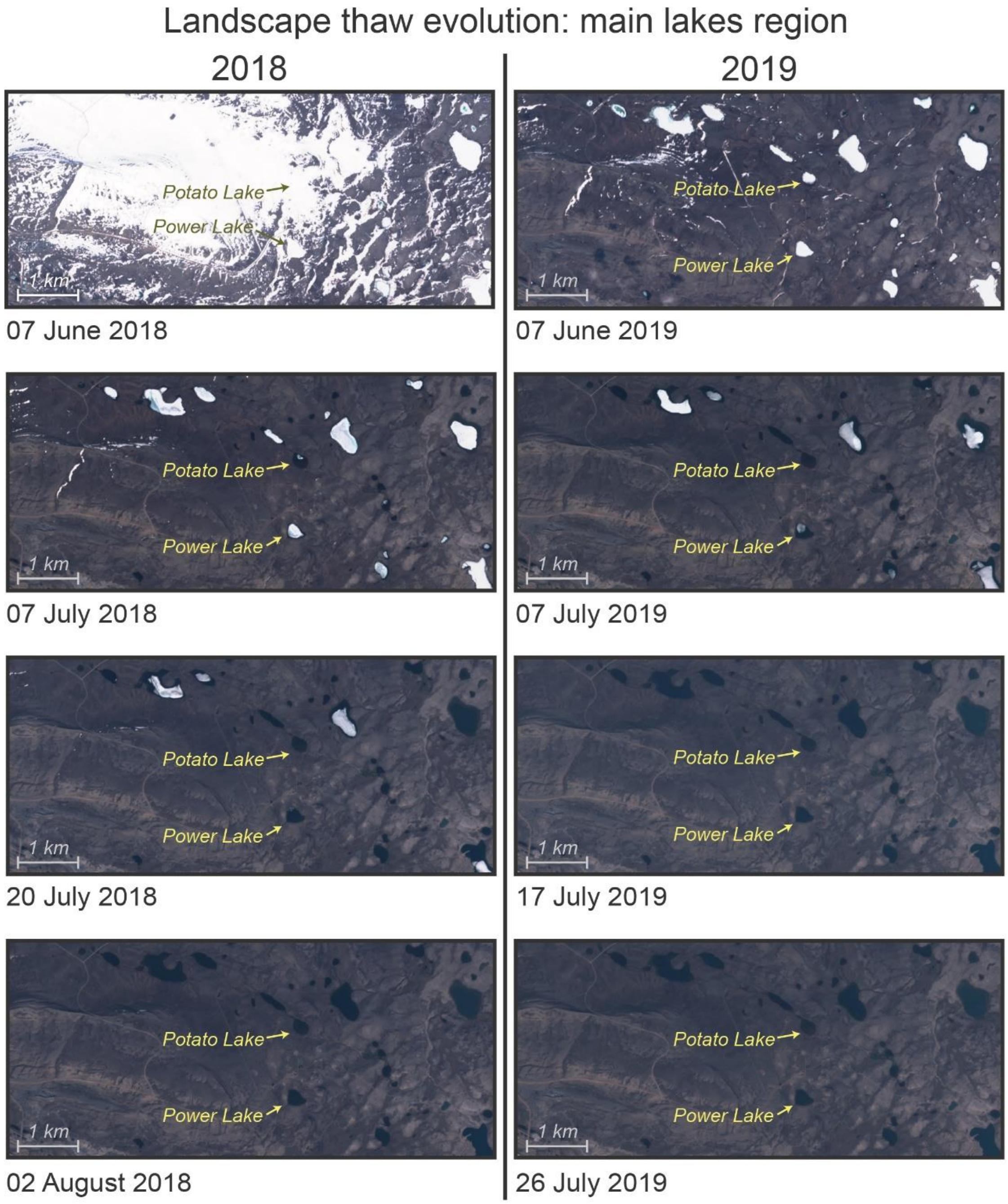

Figure S5. The general thawing progression of part of the main lakes region of the Pituffik Peninsula landscape in summers 2018 and 2019. The two frequently sampled lakes of Potato Lake and Power Lake are indicated, and other lakes can be identified through the main text's Figure 1. Photographs on the same row are matched by date across the two years, although frequent cloud cover and fog limited same day comparisons in some cases. Note that snow on the landscape and lake ice lasted later into the summer in 2018 than 2019.

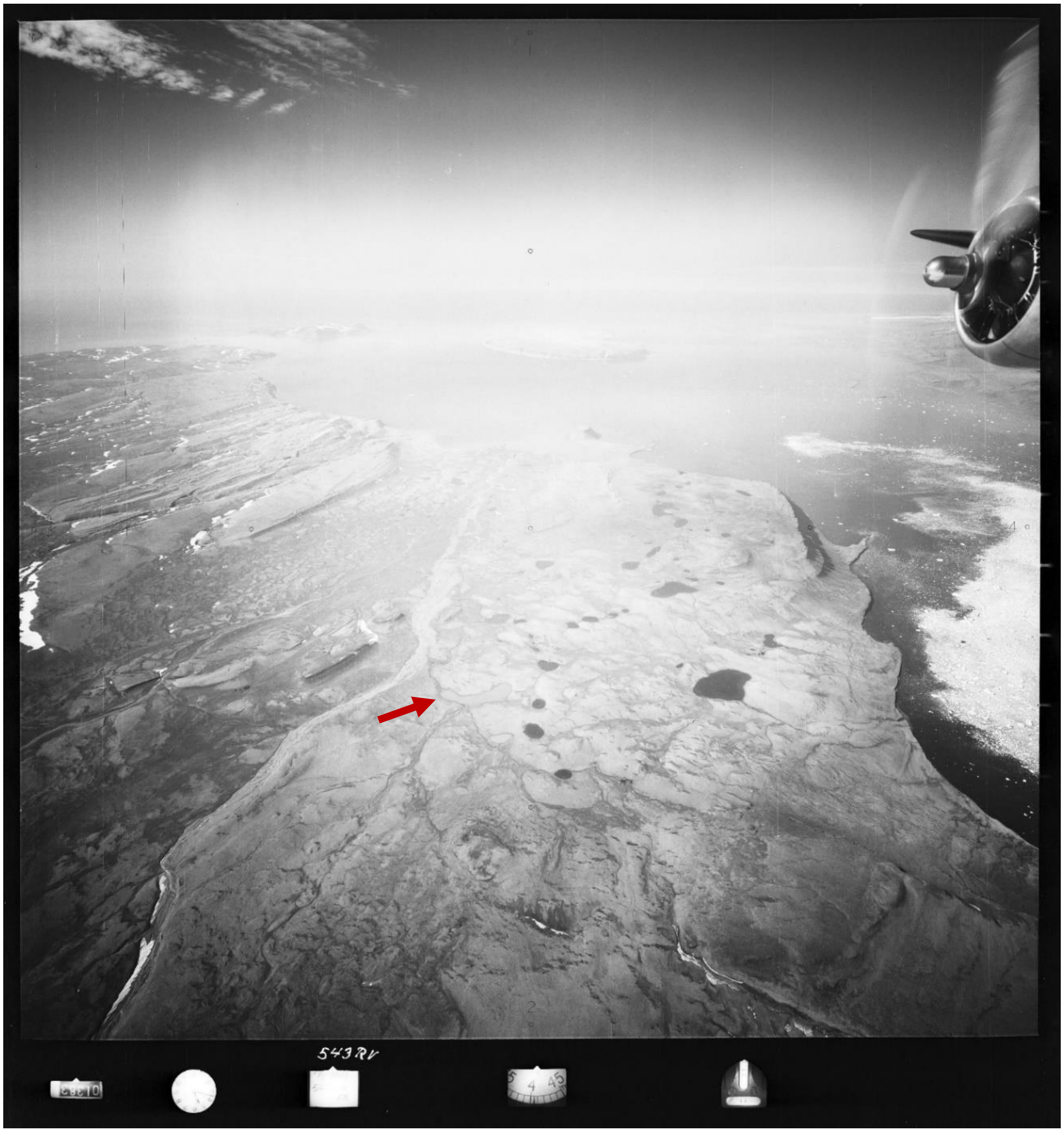

Figure S6. Aerial photograph of the main lakes region of Pituffik taken on 15 July 1949. This photograph is one of several taken on route 543RV and archived online by the Danish Agency for Data Supply and Infrastructure (Historiske Kort, 2023). The view here looks west along the northern coast of the Pituffik Peninsula from a point near the northern Tuto ice dome margin. Uummannaq can be seen just above the photograph's center, and the future Pituffik Space Base and runway will be located in the broad valley slightly left of image center. At the date this photograph was taken, the landscape and hydrology had not been significantly altered yet by humans. Of particular interest is the as-yet undammed Lake Crescent indicated by the red arrow with a notably lighter color than most other lakes in the image.

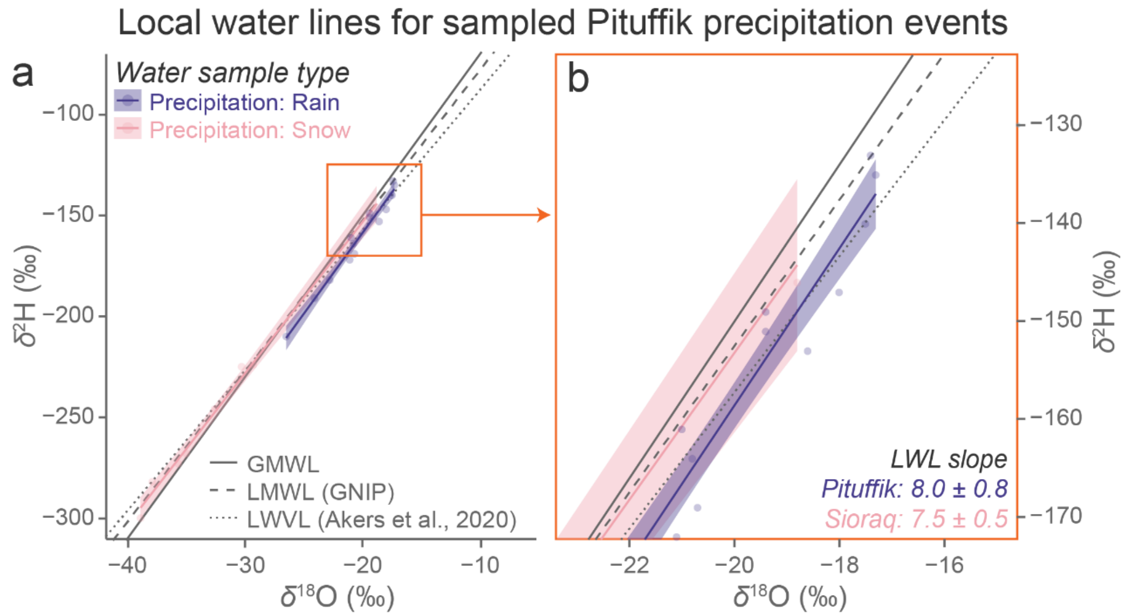

Figure S7. Local water line (LWL) linear regressions between $\delta^{18}O$ and $\delta^{2}H$ for sampled Pituffik precipitation events. Regressions are split between rain and snow events, and the 95% confidence intervals of the regressions are shaded. The global meteoric water line (GMWL, solid gray), local meteoric water line (LMWL, dashed gray) based on GNIP data (IAEA/WMO, 2022), and local water vapor line (LWVL, dotted gray) (Akers et al., 2020) are shown for reference. The plot in (b) is a magnified version of the area indicated with the orange square in (a) and matches the extent shown in the main manuscript's Figure 2c. LWL slope values and 95% confidence intervals of the slope are given at lower right.

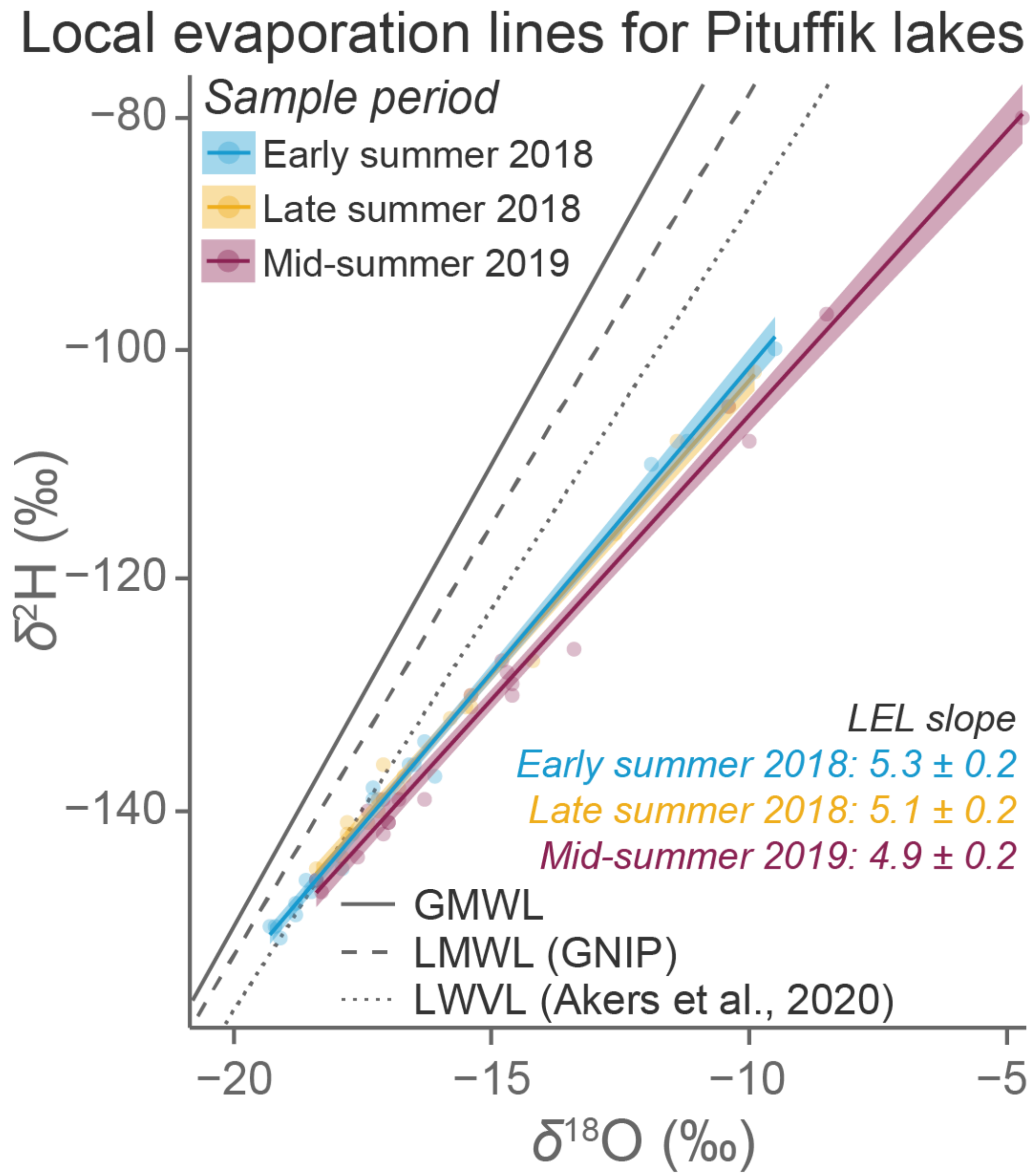

Figure S8. Linear regressions of δ^2H vs. $\delta^{18}O$ to display local evaporation lines (LELs) for Pituffik lakes by sampling period. Lake data is restricted to the subset of 18 lakes and 2 pools sampled in all three sampling periods. Each LEL represents a single sampling period and incorporates the isotopic values of all 18 lakes and 2 pools sampled during the period. LEL slope values and 95% confidence intervals of the slope are given for each sampling period at lower right. The global meteoric water line (GMWL, solid gray), local meteoric water line (LMWL, dashed gray) based on GNIP data (IAEA/WMO, 2022), and local water vapor line (LWVL, dotted gray) (Akers et al., 2020) are shown for reference.

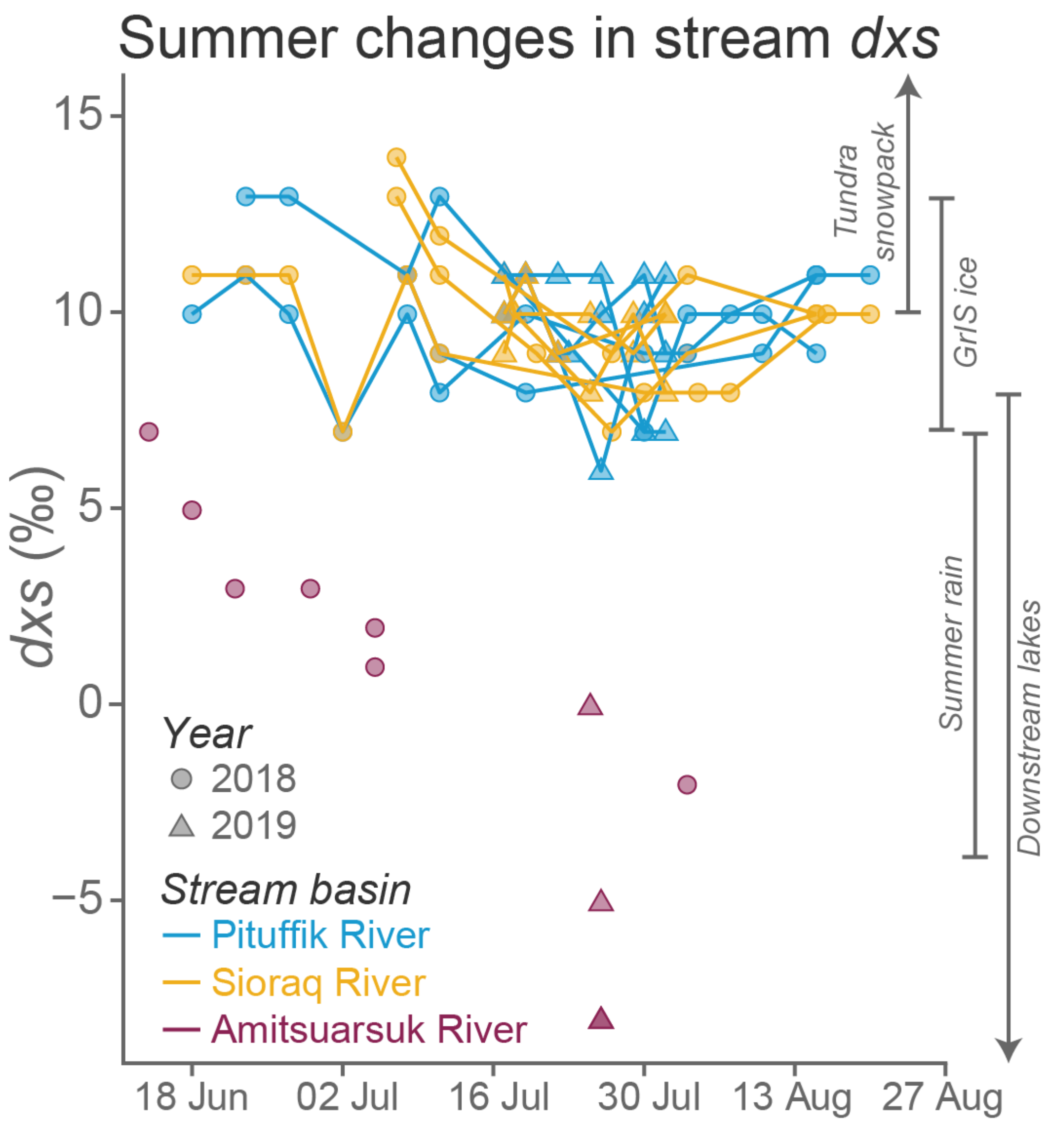

Figure S9. Evolution of Pituffik stream *dxs* values over the summer season. Samples were taken at three specific sites each along the Pituffik and Sioraq Rivers and at irregular sites along the Amitsuarsuk River. Lines connect the time-series for Pituffik and Sioraq River sites, but not for the Amitsuarsuk River because its samples were not consistently taken at the same site and thus are not a true comparable single-site time-series. Icons and lines are colored according to their stream basin. Samples from both 2018 (circles) and 2019 (triangles) are plotted by their date sampled. The *dxs* values of samples taken of the winter tundra snowpack, GrIS ice, summer rain events, and lakes with the downstream lake type are plotted at right for broader environmental context.

Table S1. Linear regression parameters for water δ^2H vs. $\delta^{18}O$ by sample type. Parameters for three isotopic reference lines are given at top: the global meteoric water line (GMWL) (Craig, 1961), the local meteoric water line (LMWL) based on monthly GNIP data taken at Thule Airport between 1966 and 1971 (IAEA/WMO, 2022), and the local water vapor line (LWVL) based on 10 min water vapor data sampled at South Mountain, Pituffik Space Base, between 2017 and 2020 (Akers et al., 2020). Parameters are given as 95% confidence intervals.

Reference line	**n**	**Slope**	**Intercept (‰)**	**r^2**
GMWL	–	8.0	+10	–
LMWL (GNIP)	42	7.5±0.4	−3±9	0.98
LWVL	147301	6.9±0.0	−18±0	0.98
Pituffik sample type				
Lake	161	5.0±0.2	−54±3	0.96
Pool	49	4.6±0.3	−63±6	0.94
Stream	121	6.2±0.3	−28±6	0.93
Surface flow	75	5.9±0.5	−36±10	0.87
Snow/ice	87	6.8±0.3	−15±7	0.95
Precipitation: rain	14	8.0±0.8	+2±16	0.97
Precipitation: snow	8	7.5±0.5	−3±16	0.99

Table S2. Results from the multiple regression and LASSO regression of lake water isotopic composition and environmental parameters. Lake sample set analyzed includes the 42 headwater and downstream lakes sampled in mid-summer 2019 and located in the main lake region north of the air base. Note that surface area was not included in the δ^2H multiple regression due to lack of importance and that LASSO regression did not find surface area or elevation to be important for δ^2H. Uncertainties are given as ± 1 standard error.

	***δ*^18^O**		***δ*^2^H**		***dxs***	
Multiple regression parameter	**Coefficient (‰)**	**p-value**	**Coefficient (‰)**	**p-value**	**Coefficient (‰)**	**p-value**
Surface area (log)	-0.39 ± 0.16	0.02	–	–	2.9 ± 0.5	<<0.001
Watershed area (log)	-0.62 ± 0.13	<<0.001	-3.8 ± 0.6	<<0.001	1.2 ± 0.4	0.002
Elevation	-0.015 ± 0.004	<<0.001	-0.068 ± 0.023	0.006	0.052 ± 0.011	<<0.001
Intercept	-1.3 ± 1.8	0.5	-74 ± 10	<<0.001	-63 ± 5	<<0.001
	Value	**p-value**	**Value**	**p-value**	**Value**	**p-value**
F-statistic	21.8	<<0.001	19.5	<<0.001	39.1	<<0.001
Adjusted r^2	0.60		0.48		0.74	
LASSO regression parameter	**Coefficient (‰)**		**Coefficient (‰)**		**Coefficient (‰)**	
Surface area (log)	-0.25		–		2.5	
Watershed area (log)	-0.43		-1.6		0.6	
Elevation	-0.006		–		0.023	
Intercept	-6.9		-116		-46	

Table S3. Slope values of daily isotopic change for Lake Potato and Power Lake. Data derived from frequent water samples taken over summer 2018.

	Lake Potato			*Power Lake*		
	$\delta^{18}O$ (‰ d^{-1})	$\delta^{2}H$ (‰ d^{-1})	*dxs* (‰ d^{-1})	$\delta^{18}O$ (‰ d^{-1})	$\delta^{2}H$ (‰ d^{-1})	*dxs* (‰ d^{-1})
Maximum	0.13	0.78	0.04	0.00	0.39	0.07
Minimum	0.00	-0.09	−0.26	0.00	0.00	−0.14
Mean ± 95% CI	0.06±0.05	0.32±0.32	−0.12±0.11	0.02±0.02	0.16±0.18	−0.04±0.07